UNCLASSIFIED

SECURITY CLASSIFICATION OF THIS PAGE *(When Data Entered)*

REPORT DOCUMENTATION PAGE		READ INSTRUCTIONS BEFORE COMPLETING FORM
1. REPORT NUMBER AFIT/CI/NR 88-88	2. GOVT ACCESSION NO.	3. RECIPIENT'S CATALOG NUMBER
4. TITLE *(and Subtitle)* TECHNIQUES IN THIN FILM FABRICATION		5. TYPE OF REPORT & PERIOD COVERED MS THESIS 6. PERFORMING ORG. REPORT NUMBER
7. AUTHOR(s) STEVEN DANE THOMPSON		8. CONTRACT OR GRANT NUMBER(s)
9. PERFORMING ORGANIZATION NAME AND ADDRESS AFIT STUDENT AT: UNIVERSITY OF FLORIDA		10. PROGRAM ELEMENT, PROJECT, TASK AREA & WORK UNIT NUMBERS
11. CONTROLLING OFFICE NAME AND ADDRESS		12. REPORT DATE 1988 13. NUMBER OF PAGES 79
14. MONITORING AGENCY NAME & ADDRESS(if different from Controlling Office) AFIT/NR Wright-Patterson AFB OH 45433-6583		15. SECURITY CLASS. (of this report) UNCLASSIFIED 15a. DECLASSIFICATION/DOWNGRADING SCHEDULE

16. DISTRIBUTION STATEMENT *(of this Report)*

DISTRIBUTED UNLIMITED: APPROVED FOR PUBLIC RELEASE

17. DISTRIBUTION STATEMENT *(of the abstract entered in Block 20, if different from Report)*

SAME AS REPORT

18. SUPPLEMENTARY NOTES

Approved for Public Release: IAW AFR 190-1
LYNN E. WOLAVER 19 July 88
Dean for Research and Professional Development
Air Force Institute of Technology
Wright-Patterson AFB OH 45433-6583

19. KEY WORDS *(Continue on reverse side if necessary and identify by block number)*

20. ABSTRACT *(Continue on reverse side if necessary and identify by block number)*

ATTACHED

DD FORM 1 JAN 73 1473 EDITION OF 1 NOV 65 IS OBSOLETE

UNCLASSIFIED

SECURITY CLASSIFICATION OF THIS PAGE *(When Data Entered)*

TECHNIQUES IN THIN FILM FABRICATION

By

Steven Dane Thompson

An improved method for preparing thin films from the plastic scintillator NE 102A is described. Detailed step-by-step instructions are given beginning with the preparation of the plastic solutions and ending with the final mounting and storage of the films. The procedure typically yields one lamination films of 45 ug/cm² thickness.

Crosslinking in NE 102A scintillator solutions was induced with Co-60 gamma rays to study the effect on physical strength of subsequent thin films. The polyvinyltoluene matrix was found to undergo crosslinking with essentially no chain scission and a gelling dose of 5.42 Mrad was determined experimentally; the G(crosslink) = 0.74. Thin films were made from NE 102A solutions which absorbed 0, 1.81, and 3.62 Mrad each. The response characteristics of each film were determined using a Cf-252 source. In general, the films from the irradiated solutions showed no evidence of diminished light output or inhomogeneity. However, films formed from the crosslinked solutions were unequivocably stronger, with strength increasing with dose.

Finally, a BaF_2 thin film was made using sedimentary techniques. The response was tested with Cf-252 fission fragments under the same conditions as the NE 102A films. The spectra were poorly resolved, but significant potential for fabricating thin films from inorganic scintillators was shown.

AUTHOR: STEVEN D THOMPSON, 1Lt, USAF

GRAD. DATE: 1987

DEGREE: M.S.

INSTITUTION: UNIVERSITY OF FLORIDA

TECHNIQUES IN THIN FILM FABRICATION

By

STEVEN DANE THOMPSON

A THESIS PRESENTED TO THE GRADUATE SCHOOL
OF THE UNIVERSITY OF FLORIDA IN PARTIAL FULFILLMENT
OF THE REQUIREMENTS FOR THE DEGREE OF
MASTER OF SCIENCE

UNIVERSITY OF FLORIDA

1987

Dedicated to my loving wife Lee Ann,

and our son Justin.

When I applied my heart to know wisdom, and to see the business that is done upon the earth (for also there is that neither day nor night seeth sleep with his eyes), then I beheld all the work of God, that man cannot find out the work that is done under the sun: because however much a man labor to seek it out, yet he shall not find it; yea moreover, though a wise man think to know it, yet shall he not be able to find it.

The Preacher

ACKNOWLEDGMENTS

This work would not have been possible if it were not for the help and support of several individuals; their assistance is therefore cheerfully acknowledged.

First, I would like to thank Dr. M. L. Muga for his invaluable help and guidance throughout the course of these investigations and subsequent preparation of this thesis. I am grateful to Dr. R. J. Hanrahan and Dr. F. E. Dunnam for their constructive suggestions offered as members of the supervisory committee.

Additionally, I am indebted to Dr. K. Williams and Chris Carrao for their tireless efforts during the conduct of the viscometric experiments. I thank Dr. A. K. Gupta for his help in using the ^{60}Co irradiator. For his expert advice and assistance in operating the thin film scintillation detector and associated data acquisition system, I thank Zoran Milosevich.

I would especially like to thank Mark Murla for his constant friendship and many helpful discussions regarding the chemistry of polymers. I am grateful to Ms. Wendy Thornton for her skill and patience in preparing the manuscript for submission to the Graduate School.

I would be remiss not to mention the cooperation and support I received from the U.S. Air Force; my assignment to the University of

Florida for the sole purpose of pursuing an advanced degree is truly appreciated.

Finally, I offer my deepest, heartfelt thanks to my wife, Lee Ann, for her continual support and encouragement.

TABLE OF CONTENTS

Page

ACKNOWLEDGMENTS iv

ABSTRACT viii

CHAPTERS

1 THIN FILM PLASTIC SCINTILLATORS 1

History of the Thin Film Detector Design 1
Response Characteristics of Thin Film Plastic Scintillators 11
Stopping Power 12
Velocity and Atomic Number 14
Film Thickness 21
Models 22
Need for Improved Thin Films 23

2 A REFINED TECHNIQUE FOR PREPARING NE 102A THIN FILMS 26

Introduction 26
Fabrication 28
Scintillator Solution 28
VYNS Solution 29
Forming the Film 29
Mounting the Film 30

3 RADIATION INDUCED CROSSLINKING OF THE POLYVINYLTOLUENE MATRIX IN NE 10ZA PLASTIC SCINTILLATOR 32

Introduction 32
Experimental 38
Calculations 43
Dosimetry 43
Molecular Weight Determination 45
G Value 50
Spectral Parameters 52
Results and Discussion 63

4 A PROTOTYPE BaF_2 THIN FILM 69

Introduction 69
Experimental 69
Results and Discussion 70

5 SUGGESTIONS FOR FURTHER WORK 74

REFERENCES 75

BIOGRAPHICAL SKETCH 79

Abstract of Thesis Presented to the Graduate School
of the University of Florida in Partial Fulfillment of the
Requirements for the Degree of Master of Science

TECHNIQUES IN THIN FILM FABRICATION

By

Steven Dane Thompson

December 1987

Chairman: M. L. Muga
Major Department: Chemistry

An improved method for preparing thin films from the plastic scintillator NE 102A is described. Detailed step-by-step instructions are given beginning with the preparation of the plastic solutions and ending with the final mounting and storage of the films. The procedure typically yields one lamination films of 45 $\mu g/cm^2$ thickness.

Crosslinking in NE 102A scintillator solutions was induced with ^{60}Co gamma rays to study the effect on physical strength of subsequent thin films. The polyvinyltoluene matrix was found to undergo crosslinking with essentially no chain scission and a gelling dose of 5.42 Mrad was determined experimentally; the G(crosslink) = 0.74. Thin films were made from NE 102A solutions which absorbed 0, 1.81, and 3.62 Mrad each. The response characteristics of each film were determined using a ^{252}Cf source. In general, the films from the irradiated solutions showed no evidence of diminished light

output or inhomogeneity. However, films formed from the crosslinked solutions were unequivocably stronger, with strength increasing with dose.

Finally, a BaF_2 thin film was made using sedimentary techniques. The response was tested with ^{252}Cf fission fragments under the same conditions as the NE 102A films. The spectra were poorly resolved, but significant potential for fabricating thin films from inorganic scintillators was shown.

CHAPTER 1
THIN FILM PLASTIC SCINTILLATORS

History of the Thin Film Detector Design

In 1970, Muga et al. [1] introduced a novel time-of-flight (TOF) particle detector which utilized an ultra-thin plastic scintillator film as a transmission detector. In this earliest thin film detector (TFD) system, the scintillator film was placed perpendicular to the face of a single photomultiplier tube and sandwiched between two lucite light guides as shown in Figure 1-1. The lucite enclosure had a large hole to permit the passage of particles and was surrounded by an aluminum can painted with optically white paint. Two such detectors, placed a known distance apart, were used in conjunction with a silicon surface barrier type solid state detector (SSD) to obtain TOF measurements; the light pulses generated by the passage of a heavy charged particle through the thin scintillator films were used to generate a timing signal which was gated by the SSD output. The experimental configuration used for recording the TOF spectrum of ^{252}Cf fission fragments is shown in Figure 1-2.

The TFD demonstrated many of the desired characteristics of an ideal transmission detector; it was reported to have a fast signal rise time of less than 5 ns and a detection efficiency of unity for fission fragments. Additionally, the minimum energy loss of the

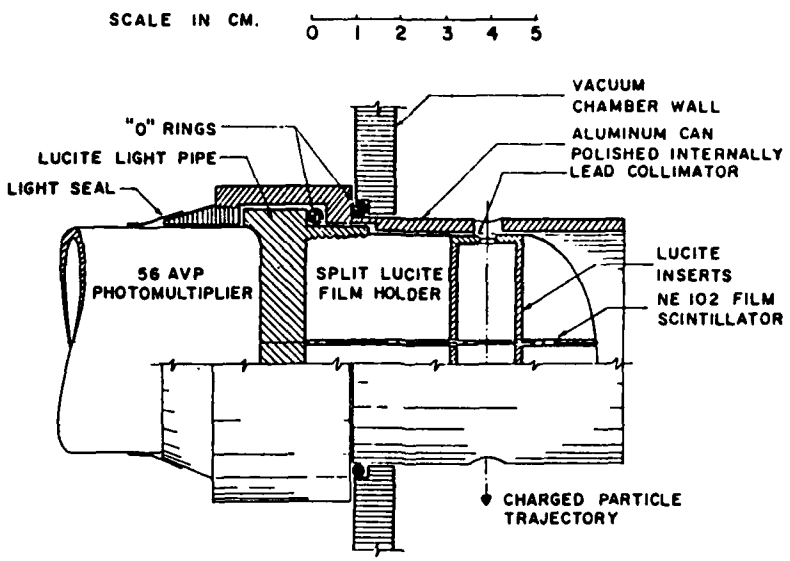

Figure 1-1 First thin film detector. Adapted from ref. [1].

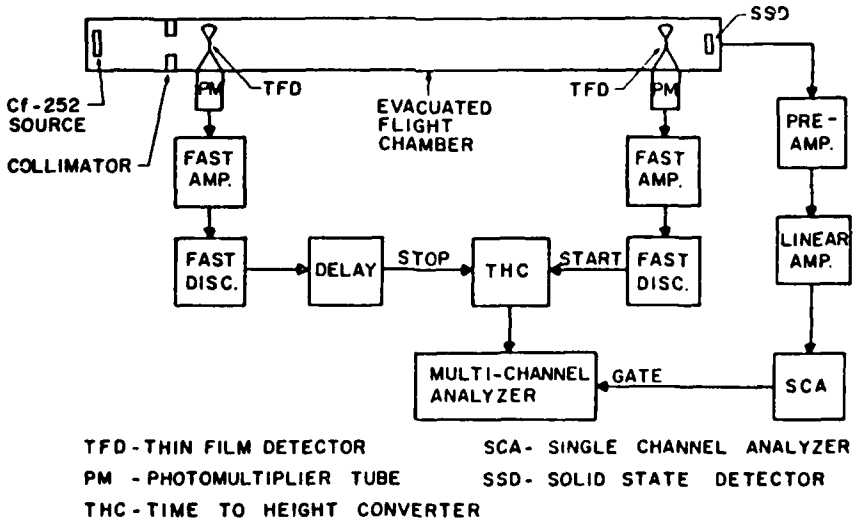

Figure 1-2 Schematic diagram of experimental assembly for recording TOF spectrum of ^{252}Cf fission fragments. Taken from ref. [1].

transient particles was found to be as small as 1% for the thinnest films ($10\mu g/cm^2$) while maintaining a quite adequate signal-to-noise ratio. It offered a relatively simple and compact system for measuring flight times of heavy atomic nuclei in comparison to the usual techniques which involved a highly charged thin metal (or metalized plastic) foil and an electron lens system [2].

Though the amplitude of the pulses generated by the scintillating film was of no real consequence in determining flight times (as long as the signals were detectable), the TFD response to the heavy and light ^{252}Cf fission fragments was notably different. This observation led Muga [3] to develop a dE/dx detector for heavy mass nuclear particles.

The new detector incorporated several improvements designed to enhance the light collection efficiency. The support for the thin film now consisted of two hemi-cylindrical lucite halves (with large holes to allow charged particles to pass) and a lucite (or teflon) sleeve coated with optical white paint, as shown in Figure 1-3. The support assembly was positioned between two opposing photomultiplier tubes whose amplifier circuits were adjusted for equal gain and shape distribution. The two amplified signals were added and then gated by the SSD output to obtain pulse height or dE/dx spectra. Figure 1-4 details the experimental configuration which was used to determine the TFD response to fission fragments.

Using the same basic set-up, Muga examined the dE/dx characteristics of the TFD response to ^{252}Cf fission fragments, accelerated ^{127}I ions, ^{3}He, and ^{4}He particles. By recording the TFD

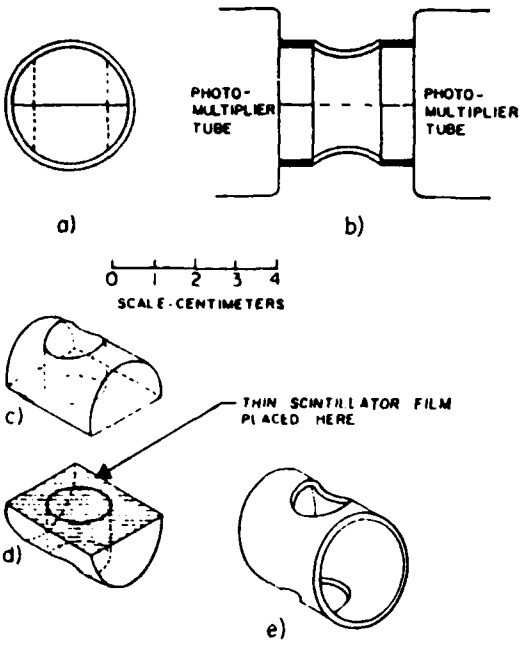

Figure 1-3 Improved TFD. The two cylindrical halves c) and d) are inserted into bushing e) after a thin scintillator film is placed on flat surface of one. Assembled unit is shown from end view a) and side (cut-away) view b). Taken from ref. [3].

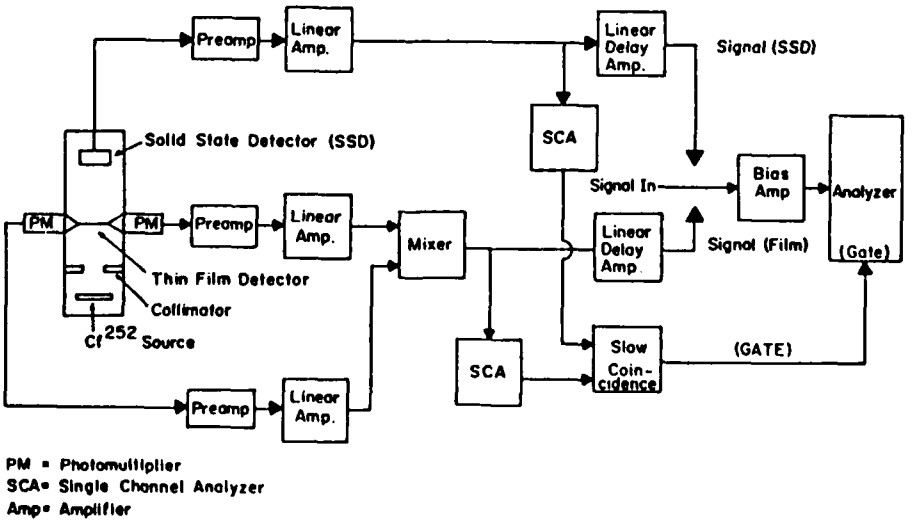

Figure 1-4 Schematic diagram of experimental set-up for testing TFD response to fission fragments as a function of residual energy measured by SSD. Taken from ref. [3].

response when gated by monotonically increasing portions of the SSD residual energy (E) peak, a correlation between the TFD pulse height spectrum and fission fragment kinetic energies was discovered; in general, a bimodal TFD spectrum which mirrored the SSD residual kinetic energy spectrum was obtained in which the more energetic light fission fragments created larger TFD signals than the typical heavy fragments. Within both groups (light and heavy) the more energetic fragments generated the larger signals. A contour plot of the TFD-SSD response to ^{252}Cf fission fragments and accelerated ^{127}I ions is presented in Figure 1-5.

The TFD response to ^{3}He and ^{4}He of comparable kinetic energies demonstrated its usefullness as a particle identifier. The energy loss (ΔE) experienced by the two types of particles when passing through the thin scintillator film was clearly discriminated.

Anticipating the possible application of the TFD for particle identification through combined ΔE, E and velocity measurements, Muga [3] conducted a series of experiments to improve TOF resolution measurements. Flight distances of 10 cm and 20 cm were compared to the 70 cm flight path used in the initial TFD system. It was found that even operating with the much shorter flight paths adequate time resolution was still maintained. Thus, essentially simultaneous measurements of ΔE, E, and velocity were shown to be feasible.

The response of thin films of varying thicknesses to energetic particles was also studied early on. In fact, in the very first TFD experiments Muga and coworkers [1] examined the ΔE spectra of ^{252}Cf fission fragments for various thicknesses of thin film scintillator

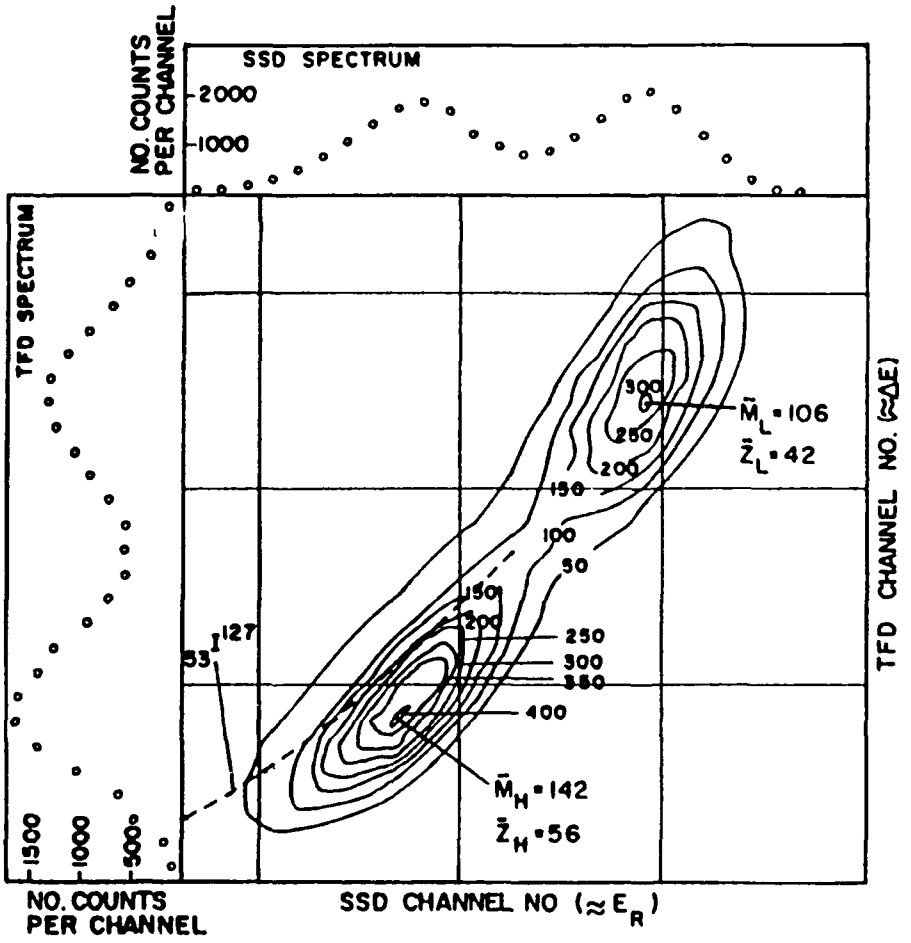

Figure 1-5 Contour plot of correlated two parameter experiment on ^{252}Cf fission fragments showing also SSD-TFD response (dashed curve) to accelerated ^{127}I ions. Inserts show the summed spectra, over TFD and SSD contours, respectively. Taken from ref. [3].

(see Figure 1-6). The energy loss of the transient particle decreased as the film was made thinner and a concomitant loss in resolution between heavy and light fragment pulse heights occurred. For film thickness of about 100 $\mu g/cm^2$, the fission fragments were degraded by 15% of the total kinetic energy and a peak-to-valley ratio (P/V) of 4 to 5 was typically achieved [3]. By "stacking" three detectors and mixing the balanced signals from all six photomultiplier amplifier circuits, Muga [3] was able to effect a significant improvement in resolution; a single detector resulted in a P/V = 4.5, two stacked together gave a P/V = 5.5 and three produced a P/V = 7.5. The summed ΔE for all three detectors was only about 40% of the total fission fragment energy. This is truly remarkable since the TFD response to total stopping of ^{252}Cf fission fragments typically yielded a P/V of about 6 to 7. This so-called stacked array of three detectors is the current configuration being utilized by Muga and coworkers in their present research endeavors. Figures 1-7 and 1-8 detail the three element TFD system and associated electronic data acquisition system used for collecting event-by-event data.

Efforts to optimize the light collecting ability, and hence the resolution, of thin film systems were initiated by several investigators [4-6]. Gelbke et al. [4] designed a TFD in which the scintillator film was supported by a wire ring and placed in a parabolic reflecting mirror. Batsch and Moszynski [5] compared the

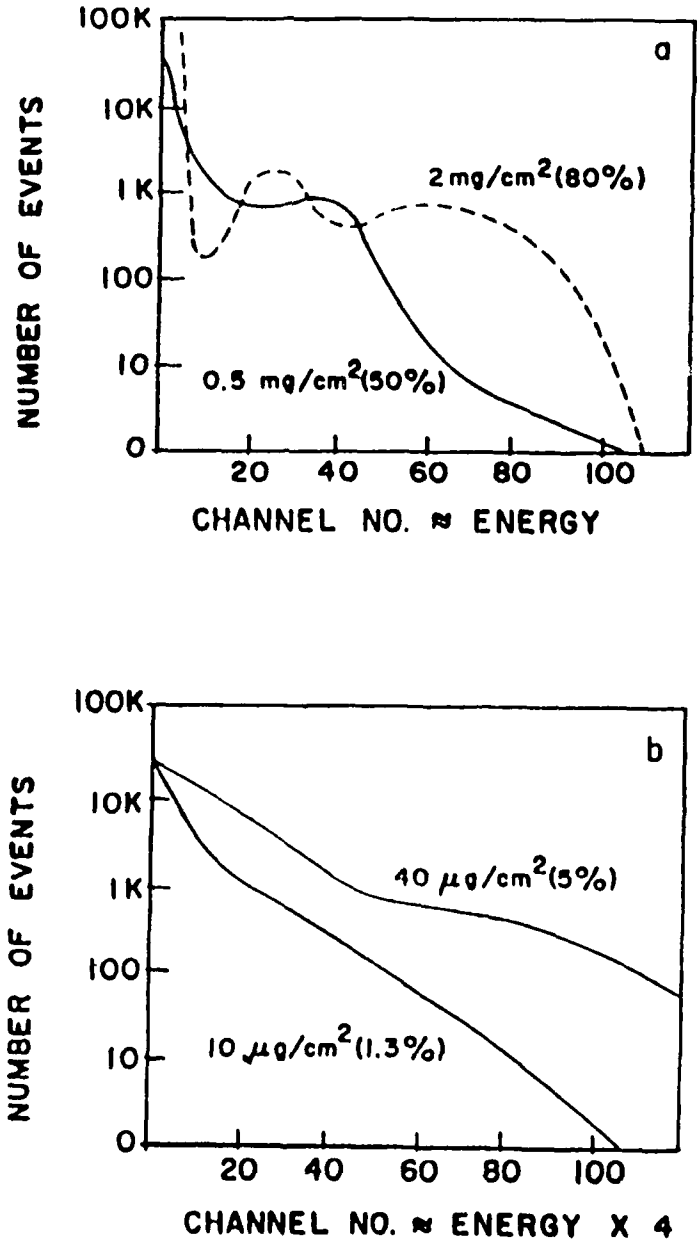

Figure 1-6 Energy loss spectrum of ^{252}Cf fission fragments passing through thin NE 102 films of various thicknesses. Number in paranthesis indicates approximate percent loss of total fragment energy. Energy scale of (b) is approximately expanded x4 relative to (a). Taken from ref. [1].

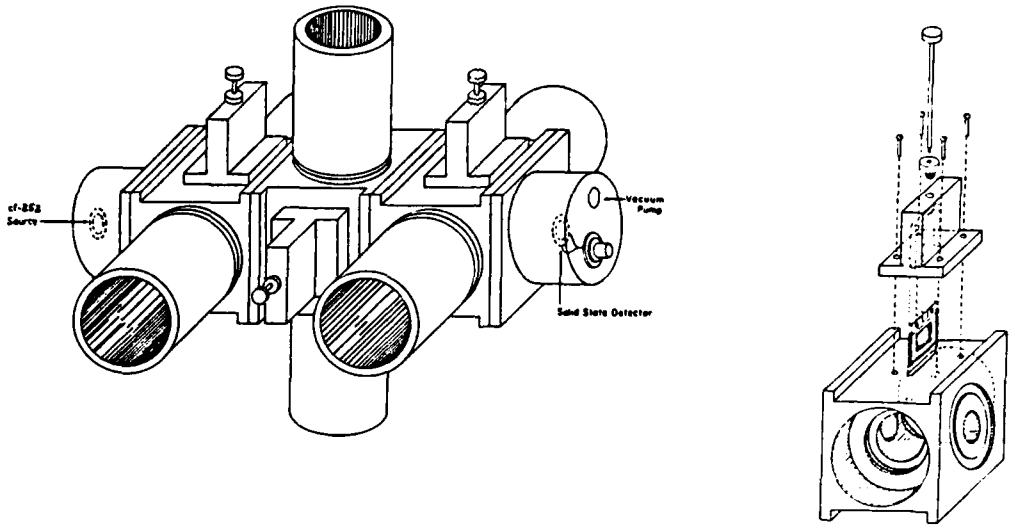

Figure 1-7 Current configuration of the Muga TFD system consisting of an array of three "stacked" detectors.

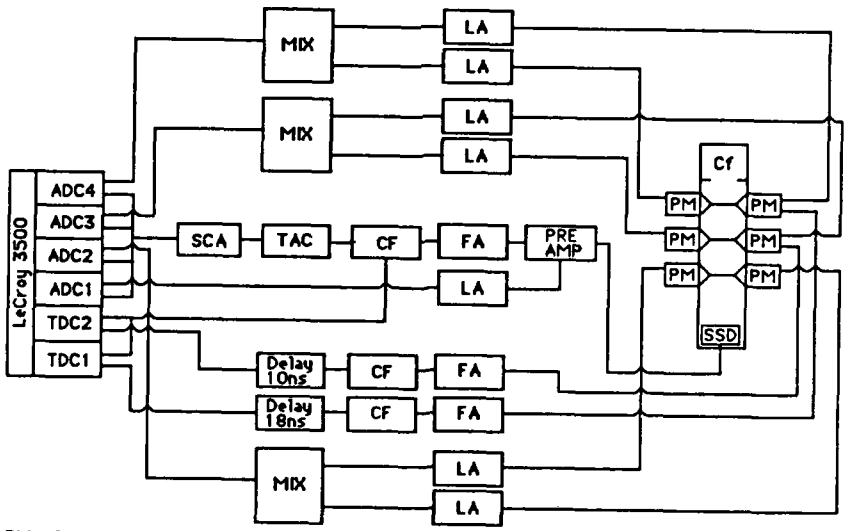

Figure 1-8 Schematic diagram of typical experimental set-up used for collecting event-by-event data.

performance of Gelbke's TFD with Muga's "light pipe" version and determined the scintillator efficiency was higher for Gelbke's detector.

Muga and Burnsed [6] also tested various light guide and scintillator film support designs for light coupl ng efficiency. Three basic thin film supports were examined: 1) two hemicylindrical Lucite "light pipes" fitted in a cylindrical sleeve (see Figure 1-3), 2) a single hemicylindrical Lucite support, and 3) a thin (0.8 mm) square celluloid frame (Figure 1-7). By masking selected portions of the photomultiplier tube faces, the amount of light reaching the exposed surfaces was revealed. The light guiding efficiency of the thin film and its support was measured by blocking off areas of the thin film surface from direct view of the photomultiplier tube faces.

Using a ^{252}Cf source and thin films of approximately 100 $\mu g/cm^2$, it was determined that less than 10% of the total light production traverses the film to emerge at the film edge. This confirmed an earlier work by Muga [7] in which a position sensitive response to alpha particles was explained through a photon collection mechanism in which the light formed is partially trapped in the thin film scintillator and guided (with exponential type transmission losses) to the photomultiplier tube face. Surprisingly, the Lucite light pipes were found to actually interfere with the light reaching the photomultiplier tube faces. The best signals were achieved using the thin celluloid frame inserted in a highly polished metal cylindrical sleeve, and it was concluded that the best light guide was the thinnest possible transparent film support.

Bendiscioli et al. [8] reported the performance of a thin scintillator detector utilizing a circular thin sheet of plastic scintillator suspended by a thin metal support within an aluminum reflecting cavity. The proportion of the light emerging from the edge of the thin scintillator disc was reported to be about 20%, which is in good agreement with the results obtained by Muga and Burnsed [6]. However, it was found that reflector surfaces coated with evaporated aluminum are much more efficient (70% higher light yield) than polished aluminum.

Undoubtedly, further improvements will be made in TFD instrument design as time progresses, and the foregoing narrative is by no means exhaustive; nevertheless, it outlines major developments leading to the present TFD design utilized in this work.

Response Characteristics of Thin Film Plastic Scintillators

The most critical component of any TFD system is the thin scintillator film. Thin film response to ionizing particles forms the basis for its utility, and the limits of resolution are ultimately determined by its scintillation properties. Since the focus of this thesis is on various techniques of fabricating thin scintillator films and their end response to ^{252}Cf fission fragments, it is appropriate to present a brief summary of the literature regarding thin film plastic scintillator response characteristics before introducing the experimental portions of this present work.

Since the advent of TFD systems nearly two decades ago, the interaction of thin film plastic scintillators with energetic ions has been studied extensively [3,5,9-24]. By far the most frequently used plastic scintillator in fabricating thin films is NE 102 [25] though NE 104, NE 110 and NE 111 have also been used [5,13,19-21]. As is readily seen from Table 1-1, the physical constants for each of these scintillators are almost identical; the only real difference lies in the emission wavelengths and decay constants. Certainly, one would expect their response characteristics to be quite similar and the aforementioned references support this conclusion. Thus, the following discussion can be applied in general to any thin film plastic scintillator.

Stopping Power

As mentioned before, Muga et al. [1] noted from the very outset that there appeared to be a relation between the energy deposited (ΔE) by a particle and the TFD response; however the exact nature of this relationship was not at all understood. To gain a better understanding of the luminescence of thin film plastic scintillators, the response of a TFD to fission fragments [3,5,9-14], accelerated heavy ions [16,19], high energy medium-heavy ions [17], and light ions [15,18,19], was studied extensively by various investigators.

In experiments involving ^{252}Cf fission fragments, accelerated ^{127}I ions, and ^{3}He and ^{4}He particles, Muga [3] demonstrated a clear

Table 1-1 Physical Constants of Plastic Scintillators

Scintillator	Base	Density	Refractive Index	Softening Point °C	Light Output (% Anthracene)	Decay Constant Main Component (ns)	Wave-Length of Maximum Emission (nm)	No. of H Atoms/ No. of C Atoms
NE 102A	PVT	1.032	1.581	75°	65	2.4	423	1.10
NE 104	PVT	1.032	1.581	75°	68	1.9	406	1.100
NE 110	PVT	1.032	1.58	75°	60	3.3	434	1.104
NE 111A	PVT	1.032	1.58	75°	55	1.6	370	1.03

dependence of the TFD response on the specific energy loss or stopping power, $\Delta E/dx$. The specific luminescence, $\Delta L/\Delta x$ (i.e. TFD response) recorded as a function of $\Delta E/\Delta x$ for hydrogen and helium ions exhibited a down-turn just before maximum energy loss was reached; Muga and Griffith [15] suggested that $\Delta L/\Delta x$ was double valued versus $\Delta E/\Delta x$. Figure 1-9 summarizes the observed trend. Muga and coworkers [16,18,20] later demonstrated unequivocally $\Delta L/\Delta x$ double valuedness using ^{4}He, ^{16}O, ^{37}Cl, ^{40}Ar, ^{79}Br, ^{81}Br, and ^{127}I ions. The TFD response to ^{4}He is shown in Figure 1-10. Becchetti et al. [19] observed the same trend for a range of different ions from H to Br. Their values of $\Delta L/\Delta x$ versus $\Delta E/\Delta x$ are shown in Figure 1-11. Thus the TFD response, which is directly proportional to the specific luminescence, is not a simple function of the specific energy loss.

Velocity and Atomic Number

A considerable amount of experimental evidence [3,12,15-17] has been collected which shows TFD response depends predominantly on two elementary variables, namely, the velocity and the atomic number(Z) of the transiting ion. Muga [3] measured the TFD response to degraded fission fragments as a function of average fragment kinetic energy, and as a function of average fragment velocity. Figure 1-12 shows the quite different TFD pulse heights obtained for the light fragments compared to the heavy fragments. Since the two groups were clearly resolved, a dependence on the mass(m), Z, or velocity was

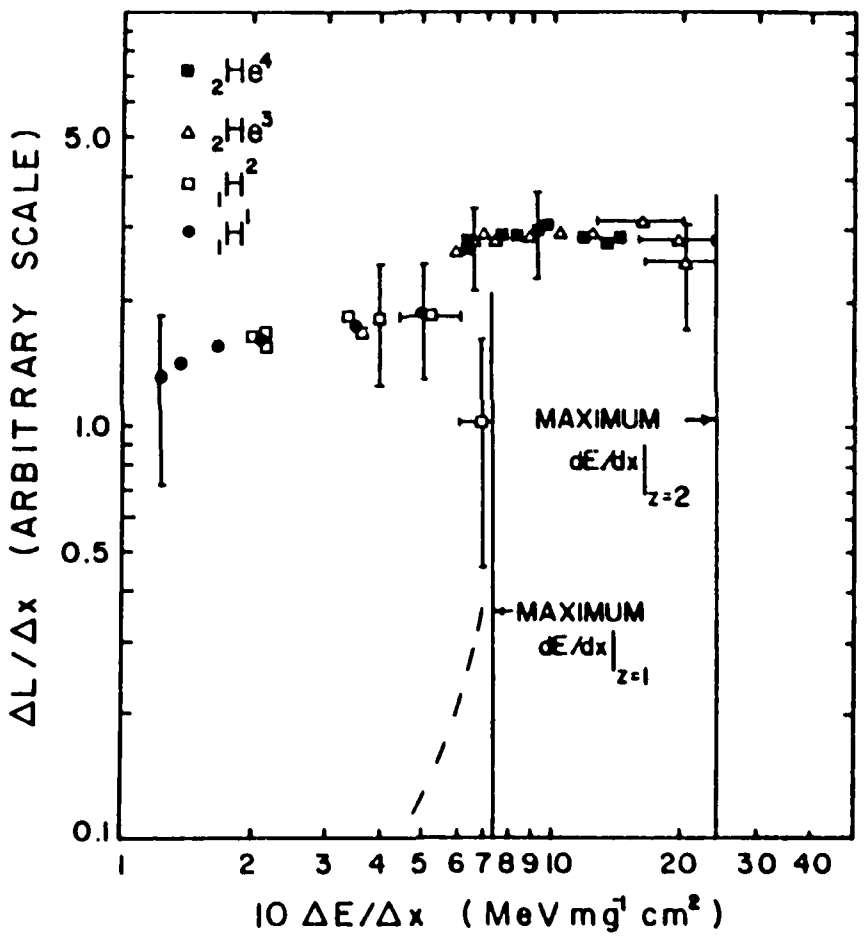

Figure 1-9 Specfic luminescence as a function of specific energy loss for incident light ions. The limit bars represent fwhm values for the TFD pulse height distribution. Taken from ref. [21].

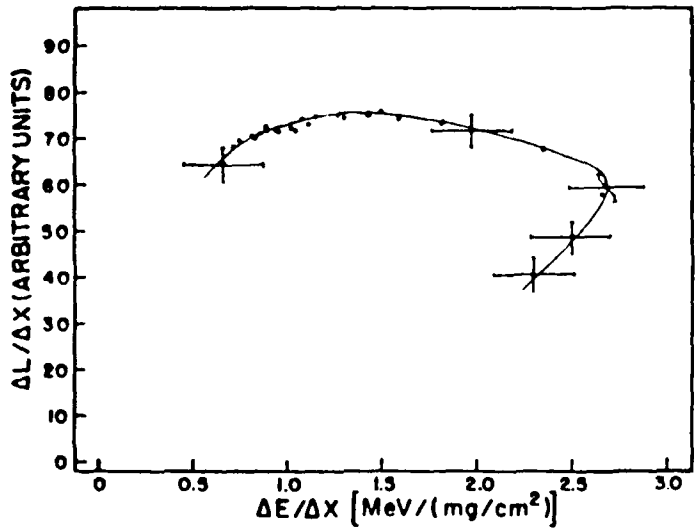

Figure 1-10 Specific luminescence as a function of specific energy loss for ^{4}He ions transiting 112 μg/cm² NE 102 scintillator. Taken from Ref. [18].

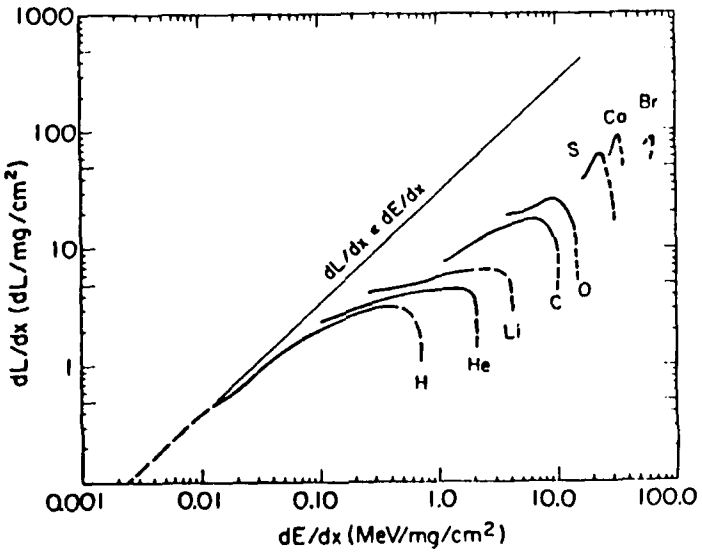

Figure 1-11 Specfic fluorescence vs. calculated specific energy loss in NE 102 for selected light and heavy ions. Taken from ref. [19].

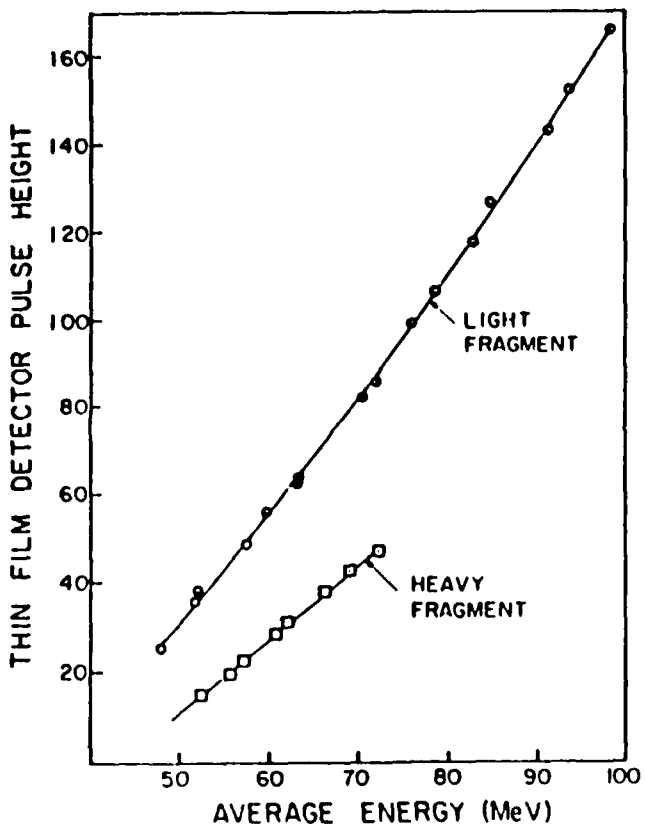

Figure 1-12 TFD response to degraded fission fragments as a function of average fragment kinetic energy. Taken from ref. [3].

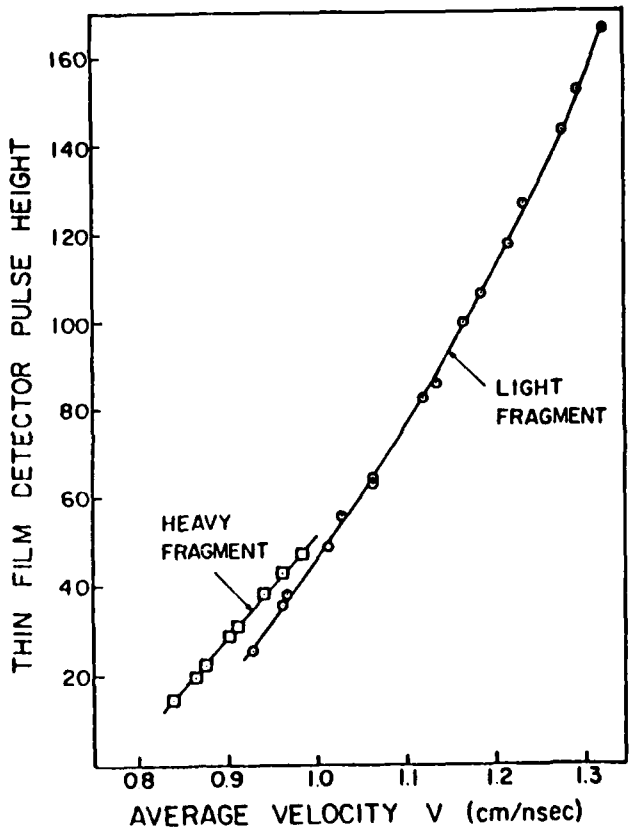

Figure 1-13 TFD response to degraded fission fragments as a function of average fragment velocity. Taken from ref. [3].

strongly suggested. The TFD response as a function of average velocity is shown in Figure 1-13 and the velocity effect on pulse height is apparent; an increase in TFD response with increasing particle velocities is observed, which is in agreement with higher TFD response for light fragments versus heavy fragments (Figure 1-12) at equivalent energies. Nevertheless, the two fragment groups still displayed disimilar responses even at the same velocities. An additional dependence on m and/or Z was now very likely.

In further experiments with ^{4}He, ^{3}He, ^{2}H, and ^{1}H ions, Muga and Griffith [15] demonstrated a clear Z dependence and mass non-dependence of the TFD response. As with the fission fragment experiment, the TFD response, recorded as a function of ion energy, yielded a distinguishably different curve for each of the light ions. The results are displayed in Figure 1-14, and as before, a dependence on one (or some combination) of the variables m, z, and velocity is intimated. However, when the TFD response as a function of ion velocity was measured, the isotopic pairs ^{3}H, ^{4}He and ^{1}H, ^{2}H were coincident; the Z dependence was thus substantiated and the results are shown in Figure 1-15.

Using accelerated heavy ions, Muga et al. [16] again showed the dependence of the TFD response on the nuclear charge Z and ion velocity. When plotted as a function of the incident ion's energy per nucleon, the TFD response takes the shape of a family of curves as shown in Figure 1-16. Figure 1-17 shows the family of velocity (energy per nucleon) curves when the thin film response is plotted as a function of nuclear charge. The slopes of these curves indicate

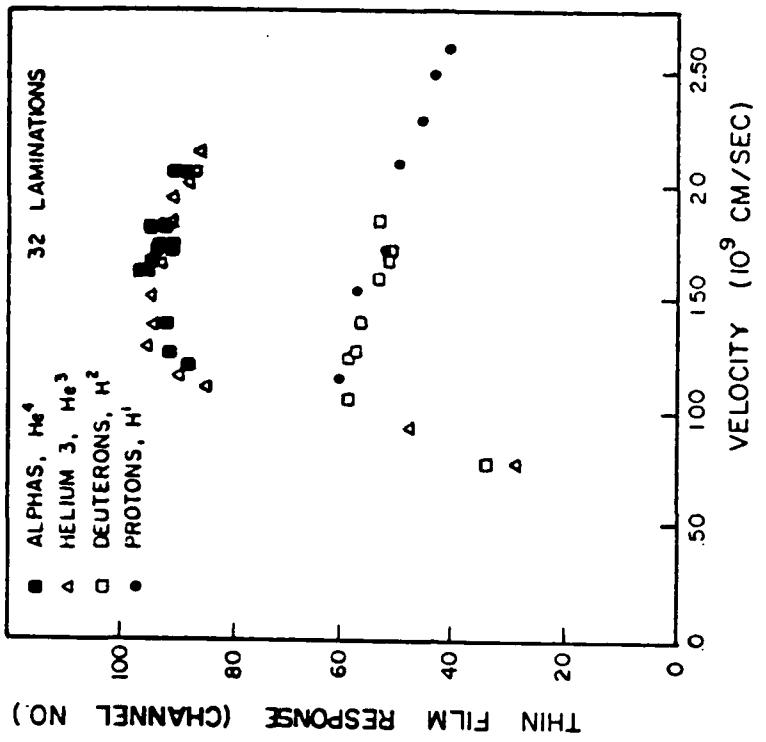

Figure 1-15 TFD response as a function of ion velocity. Taken from ref. [15].

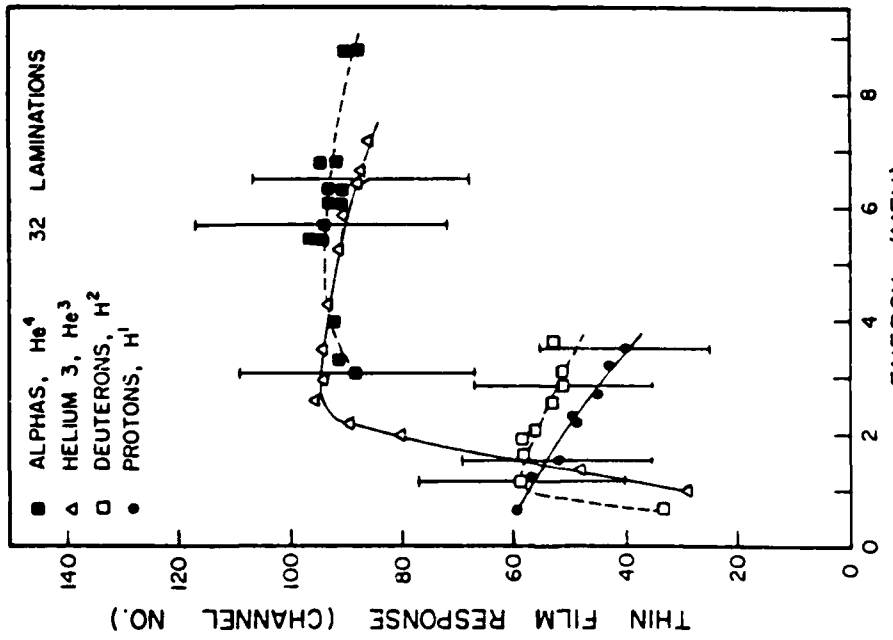

Figure 1-14 TFD response as a function of ion energy. The limit bars indicate fwhm of pulse height distribution. Taken from ref. [15].

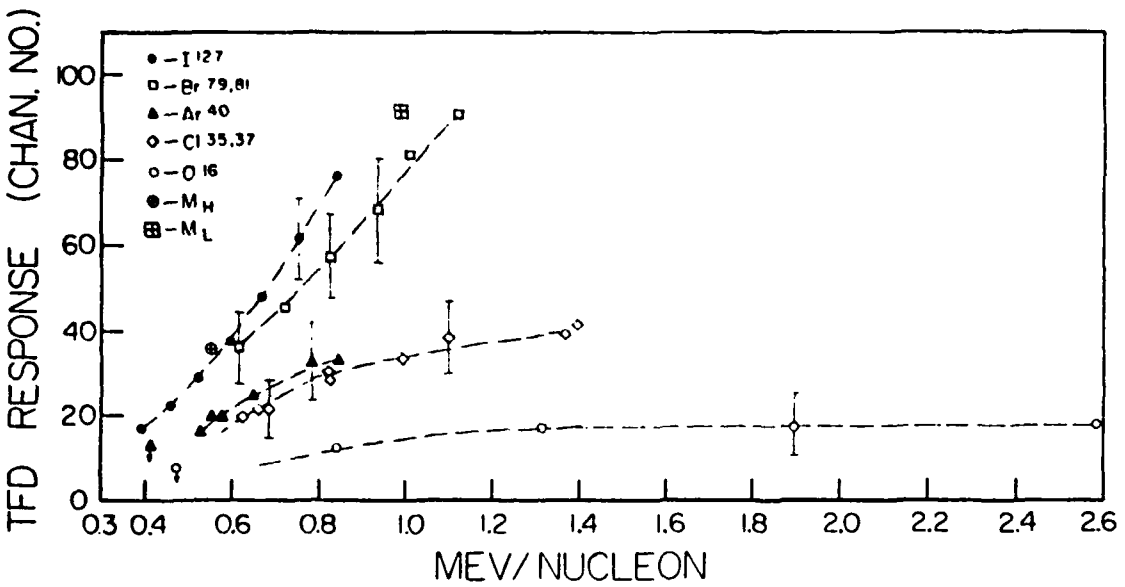

Figure 1-16 TFD response vs. energy/nucleon of incident ion. Limit bars indicate fwhm of pulse height distributions. M_H and M_L refer respectively to mean heavy- and light-mass ^{252}Cf fission fragments. Taken from ref. [16].

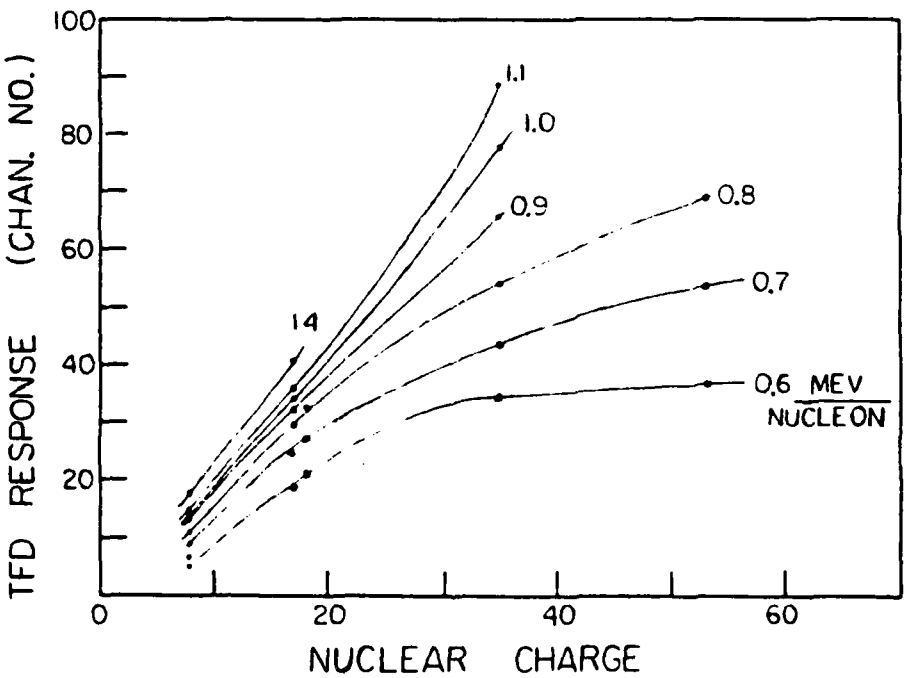

Figure 1-17 TDF response as a function of nuclear charge of transiting ion for given values of energy per nucleon. Taken from ref. [16].

the sensitivity of the thin film response to a variation in charge; the greater the slope, the greater will be the charge differentiation. Based on these curves, the charge on heavy ions is better resolved at higher velocities.

Film Thickness

The effect of scintillator thickness on TFD response has also been investigated [5,10-14]. Of course, varying the thickness of the film and then observing the TFD response is essentially the same as measuring the specific luminescence (TFD response) as a function of specific energy loss (stopping power) which has already been discussed. However, several interesting observations have resulted from these studies.

Batsch and Moszynski [5] observed that ultra-thin foils (<300 $\mu g/cm^2$) made from a ternary solution scintillator (e.g. NE 102) behave as a binary one; the secondary fluor added to serve as a wavelength shifter plays no role in the light generation process.

Batra and Shotter [10] investigated the influence of the laminated structure of thin films on response to fission fragments. They found the spectrum of ^{252}Cf recorded from a film of three laminations (thickness ≈ 1.16 mg/cm^2) was slightly shifted to higher channels (≈ 5%) as compared with that recorded by a single film (thickness ≈ 1.2 mg/cm^2). The resolution measured by the P/V was practically the same. The slightly higher pulse height for the laminated structure as compared to the single film response was attributed to better transmission of the scintillations produced in the multilayers of the laminated film.

Batsch and Moszynski [5] found a decrease in scintillation efficiency in ultra-thin foils and attributed this effect to surface quenching. Brooks et al. [12] reported that when the TFD thickness is decreased, a critical thickness dependent on the range of the non-radiative energy process in the plastic is eventually reached. Below this thickness the TFD characteristics are dominated by the properties of the surface regions, which show a poorer scintillation efficiency than the inner region of thicker thin films. They further suggested that surface properties and nonradiative transfer processes may be sensitive to the method used to prepare the thin film.

Manduchi et al. [13] observed occasional large variations in TFD response for thin films of similar thickness and cited an inherent problem of consistently producing thin films with the same properties as a possible reason.

Models

The scintillation process in organic scintillators (e.g. plastic scintillators) has been described quite well in a review article by F. D. Brooks [26]. As a heavily ionizing particle passes through the scintillator medium, molecules up to several molecular diameters from the particle path are ionized or excited by direct Coulomb interaction (primary excitation). Secondary electrons released by close encounters with the particle cause further excitation as they are stopped in the medium. The density of excitation drops off away from the particle path but a core or track of very high excitation density can be defined

extending a radius r_o about the particle trajectory as shown in Figure 1-18. The escape of fast secondary electrons (δ-rays) from the track results in further excitation and ionization outside of the track, including additional localized regions of high excitation density called "blobs" and "spurs." A very heavily ionizing particle produces a high density of δ-rays and consequently the blobs and spurs outside the track merge to form a more or less uniform annular region of high excitation density. Of course the density of primary excitation in the track and beyond it depends on $\Delta E/\Delta x$, Z and the velocity of the particle.

For plastic scintillators (which are generally binary or ternary systems) the incident ionizing particle deposits energy essentially entirely in the bulk consistuent or solvent, but through efficient energy transfer from solvent to solute (fluor), the final luminescence originates almost entirely from the fluor.

From this basic mechanism, several mathematical models have been proposed. Three particularly successful models have been proposed by Muga et al. [21,22], Ajitanand [23], and Kanno and Nakagome [24].

Need for Improved Thin Films

Thin film systems have been successfully employed in a variety of experimental situations [1,26,28-31] and have been suggested for use in many others [3,31]. One particularly exciting application is as an event-by-event particle detector. Muga et al. [31] have recorded large numbers of events for ^{252}Cf fission fragments and selected heavy ions. They report that an explicit algorithm relating ion velocity and $\Delta L/\Delta x$

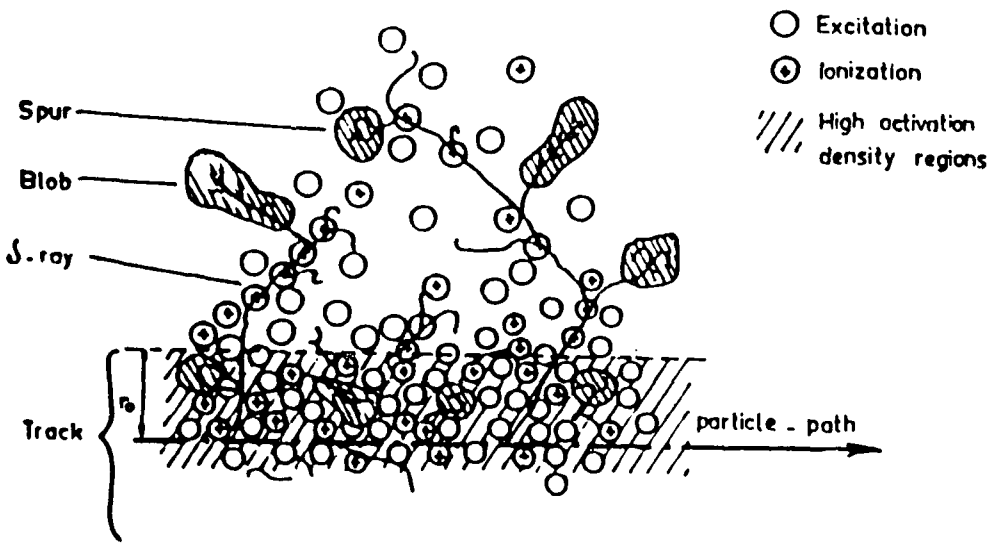

Figure 1-18 Schematic representation of spatial distribution of activations induced by a charged particle. Taken from ref. [27].

to nuclear charge Z is expected soon. Thus, with TOF and $\Delta L/\Delta x$ measurements used to identify Z, and E from the SSD with coincident velocity measurements used to establish m, utility as a particle identifier appears imminent.

However, in order to realize this objective techniques for reproducibly fabricating scintillator films with extremely high resolution characteristics must be developed. It was this need for better thin films that provided the motivation for this work.

CHAPTER 2
A REFINED TECHNIQUE FOR PREPARING NE 102A THIN FILMS

Introduction

Since the performance of the scintillator film ultimately determines the limits of resolution obtainable for any TFD, system the development of methods for reproducibly making films of uniform thickness, smoothness, clarity, etc. is of paramount importance. This critical relationship between the TFD response and the way in which the scintillator film is prepared is certainly worthy of close scrutiny.

Muga et al. [32] described a "recipe" for making thin NE 102 films which has served as the basis for currently used techniques. The procedure entails the mixing of an ester solution of the plastic scintillator and the subsequent film formation by flowing a few drops of the scintillator solution over the surface of distilled water. The films are lifted using a wire ring with stem and are lowered down onto the film support. Increased thicknesses of film are made by placing additional films one-by-one onto the film support. Also described is a process for sandwiching the laminated scintillator films between two protective VYNS [33] films and a final heat treatment to "weld" the scintillator film to the support.

Batra and Shotter [10] have suggested a slightly different procedure for making thin films. The solution of plastic

scintillator is prepared in the same manner as prescribed by Muga et al. [32], but an "O-ring" is floated on the surface of the water to help stretch the water surface, and thus permit the scintillator solution to spread more uniformly over the stretched surface. Film thickness is controlled by adjusting the concentration of the scintillator solution and the number of drops added.

A quite different technique was introduced by Goldstone et al. [34] and has been used widely [13,35,36] with minor modifications. This technique requires the plastic scintillator be dissolved in toluene and the resulting solution spread on a level glass surface; the solvent is then allowed to evaporate in a dust-free area. When all of the solvent has evaporated, the film is floated off of the glass slide in deionized water and then removed from the water on a wire frame. Thickness is controlled by varying the amount of scintillator in solution and the area over which the solution is spread.

The procedure which follows is essentially a refinement of the method introduced by Muga et al. [32]; the scintillator solution composition was optimized for flow characteristics and resultant thin film strength, and the procedure for forming and mounting the thin films is a synthesis of practical techniques developed by Muga and his graduate assistants over the years.

Fabrication

Scintillator Solution

The scintillator solution is prepared by adding 12 g of NE 102A plastic scintillator chips to a solution of 50 mL ethyl acetate and 2.2 mL amyl acetate in a tight-sealing glass or polyethylene vessel (short chain esters are quite volatile). Since this mixture represents a nearly saturated solution of NE 102A (which is >96% high polymer polyvinyltoluene), complete dissolution occurs but slowly even with frequent, vigorous stirring. The solution typically requires about a week to form a completely homogeneous mixture. Bilaminar flow while stirring is indicative of continued extensive aggregation of the polymer coiled chains and is an obvious sign of incomplete equilibration.

After an adequate amount of time, the solution can be transferred to a polyethylene squeeze type drop dispenser equipped with a friction-fitting closure. Though dropper bottles are certainly convenient, the drop spout tends to clog frequently with hardened plastic scintillator. Perhaps a better method is to store the scintillator solution in the original vessel and use disposable Pasteur pipets to withdraw and dispense the solution. Of course, the advantage lies in the fact that the pipets are very inexpensive and can be discarded after each use.

VYNS Solution

VYNS is a very tough resin made of a polyvinylacetate-polyvinyl chloride copolymer. The VYNS solution is made by dissolving 4.0 g of VYNS plastic in 50 mL of cyclohexanone. Again, a tight-sealing glass or polyethylene container should be used because of the high vapor pressure of the solvent. With frequent stirring, the VYNS will completely dissolve in about 24 hours. A polyethylene dropper bottle is recommended for storing and dispensing the solution (clogging of the drop spout is not a problem).

Forming the Film

The thin plastic film is formed by using a technique commonly employed in preparing plastic target backings [37]. A porcelain pan (5 cm x 30 cm x 50 cm) is filled approximately half-way with deionized water. A ground-glass plate is partially immersed in the water and leaned against one end of the pan at about a 45° angle. A second glass plate is submerged and butted against the foot of the inclined plate to help hold it stationary. A bead of plastic solution is dispensed across the glass plate, immediately above the water line. When this line of solution touches the water, the plastic quickly flows across the surface. The hydrophilic solvent rapidly enters the aqueous phase leaving behind a smooth solid plastic film. Interference color patterns are typically seen in NE 102A films--especially near the fringes. A section without blemishes and of approximately uniform color should be chosen for use in constructing the TFD.

Mounting the Film

An 8 cm diameter ring with a stem is used for lifting the films from the water. The tool is made from stiff wire and the ring portion is wrapped by hand with numerous layers of NE 102A or VYNS film to aid in adhesion of the film. The film is lifted from the water surface by gently placing the wire ring onto the selected portion of floating film. The ring is then rotated gently through several revolutions to cause the film outside the ring to stick. Then the wire ring and film are tilted slightly as the assembly is drawn across the water to gently break the surface tension, and the film is lifted way. Since both NE 102A and VYNS films shrink appreciably upon drying, the ring/film assembly is held in the air for about 30 seconds to prevent stress cracking after mounting. During this time the film can be examined closely for any blemishes or tears. Since freshly made films generally carry a small static charge, it is important the process be carried out in a clean, dust-free environment.

The film is mounted on a thin, square celluloid frame, 2.8 cm on a side with a 2.0 cm square cut out of the center. The frame is positioned on a hollow cylindrical stand (i.d. = 3.5 cm, o.d. = 4.5 cm, height = 6.0 cm) for ease in mounting. The film is transferred to the celluloid frame by gently bringing the ring/film assembly down squarely over it. The outside portion of the film is then cut away with a scalpel or torn away by further downward motion of the wire

ring. A VYNS film will adhere quite well to the celluloid frame, and an NE 102A film will adhere to a VYNS film (or another NE 102A film). An NE 102A film can (if protective VYNS layers are not desired) also be affixed directly to the celluloid frame by applying a very thin coat of silicone grease to the frame prior to mounting.

VYNS films typically have an areal density of about 10 $\mu g/cm^2$. A single NE 102A film is approximately 45 $\mu g/cm^2$ thick. Increased scintillator thicknesses are obtained by placing additional NE 102A films one-by-one onto the frame. However, in order to prevent trapping air pockets between the laminations, the ring/film assembly is lowered at a slight tilt and the new film allowed to sweep smoothly across the previously mounted film layers.

The scintillator films are normally sandwiched between two VYNS films by forming the first and last film layers from the VYNS solution. The VYNS films provide physical support for the much more fragile NE 102A layers, and form a protective layer to help reduce thin film response shift with the passage of time. Bendiscioli et al. [8] reported a 30% loss in scintillator efficiency per year for unprotected films stored in air. They concluded the decrease was due to the quenching effect of oxygen molecules deposited on the surfaces, and suggested storing the scintillators in a vacuum or under nitrogen. By utilizing the VYNS technique, the internal scintillator films are protected from atmospheric effects and can be conveniently stored in an ordinary desiccator. Of course, the disadvantage of using VYNS films is that they degrade the energy of the transiting ions without contributing to the light output.

CHAPTER 3
RADIATION INDUCED CROSSLINKING OF THE POLYVINYLTOLUENE MATRIX IN NE 102A PLASTIC SCINTILLATOR

Introduction

Even though the technique described in Chapter 2 for preparing thin films is quite successful, the procedure for mounting the films is rather tedious. Since several laminations are typically needed to achieve the required areal density (commonly 100-300 $\mu g/cm^2$) a film is often ruptured while attempting to lay down an additional layer necessitating the entire mounting process to be started over from the start. Simply stated, the films lack substantial physical strength and a tremendous savings in preparation time could be achieved if stronger thin films could be made.

A very common method used for changing the physical properties of a polymer is to expose it to radiation [38]. Of particular interest is the fact that only small chemical changes, such as are produced by moderate doses of radiation, cause large changes in the physical properties of some polymers. The main chemical changes taking place upon irradiation can be divided into two classes: crosslinking and degradation [38-43].

Crosslinking is a process whereby separate polymer chains become linked together. It leads to an increase in the average molecular weight and degree of branching and, at high enough doses, results in the formation of a three-dimensional network or gel consisting of

essentially one giant molecule. By controlling the dose, the average molecular weight of the material can be selectively increased. Since most important mechanical properties improve considerably with increasing molecular weight, irradiation of polymers which predominantly crosslink is a useful technique for increasing their temperature resistance, dimensional stability, mechanical strength and clarity [38,43,44].

Degradation or scission results when the molecular chains are fractured causing a reduction in the average molecular weight. Generally, both crosslinking and degradation may occur to a limited extent at the same time, but the net effect depends on which is predominant. Both processes are thought to involve the formation of free radicals, and the differing susceptibilities to scission and crosslinking exhibited by various polymer structures are usually explained in terms of free radical reactions [41-43].

A rough guide for predicting which polymers will degrade and which will crosslink has been developed [45]; polymers containing two side chains attached to a single carbon (e.g. $-CH_2-CR_1R_2-$) degrade while those with a single side chain or no side chain (e.g. $-CH_2-CHR_1-$ or $-CH_2-CH_2-$) crosslink. Unfortunately, the tendency to crosslink or degrade is not just a function of polymer structure, but also of the experimental conditions employed during irradiation. For example, the presence of oxygen tends to encourage scission in some polymers. Also solutions of polymers are influenced by the nature of the solvent used as well as the concentration of polymer present [40, 41,43].

The NE 102A plastic scintillator is a ternary solution of p-terphenyl, 1,4-bis-[2-(5-phenyl-oxazolyl)]-benzene (POPOP) and polyvinyltoluene (PVT). The PVT polymer matrix is by far the major constituent (>96%), thus irradiation of the scintillator solution described in Chapter 2 might be a plausible method for increasing the average molecular weight--and correspondingly, the strength of the resulting thin films. Also referred to as polymethylstyrene, PVT is a vinyl polymer containing one α-hydrogen to the $-CH_2-$ group and thus meets the empirical criterion set forth for crosslinking polymers.

Because PVT differs from polystyrene only by the presence of a methyl group on the benzene ring, their responses to radiation should be quite similar. The behavior of polystyrene in organic solutions has been studied extensively [46-53]. Wall and Magat [46], observed a decrease in dilute (2 to 4%) polystyrene solutions irradiated in air and interpreted the effect as being due to an oxidative degradation of the polymer initiated by the free radicals generated in the radiolysis of the solvent. Chapiro et al. [47] and Durup [48-51] also studied the oxidative degradation of polystyrene in solution. Henglein and Schneider [52,53] found the rate of degradation of 1% polystyrene solutions in different solvents increases in all cases when the irradiations are carried out in the presence of oxygen; however, degradation was still the predominant effect even in the absence of oxygen (see Figure 3-1). It should be mentioned at this point that if diffusion is very slow compared to radical formation (or if the vessel containing the solution is sealed), all the oxygen initially dissolved should be rapidly

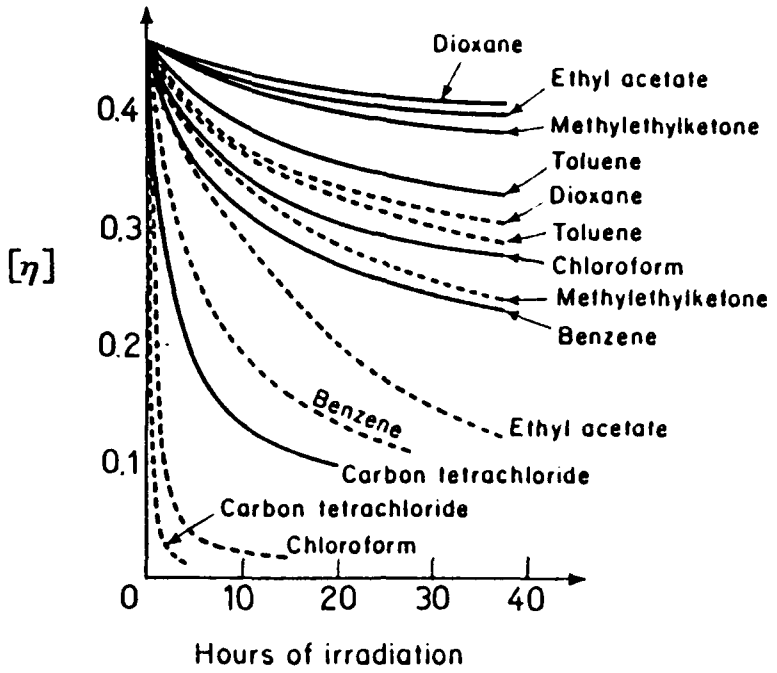

Figure 3-1 Influence of dose on the intrinsic viscosity of polystyrene iradiated in 1% solutions of various solvents. Solid curves: irradiations under argon; broken curves: irradiations with continuous bubbling of pure oxygen through the solution. Taken from ref. [43].

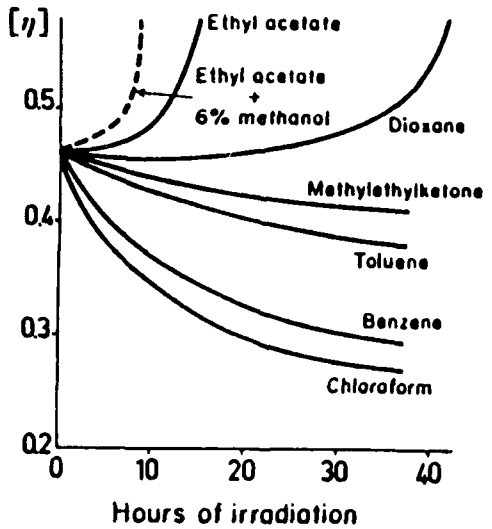

Figure 3-2 Influence of gamma ray dose on the intrinsic viscosity of polystyrene irradiated in 5% solutions in various de-aerated solvents. Taken from ref. [43].

consumed, and thereafter the reaction within the polymer solution should proceed as though irradiated in vacuo [42].

Henglein and Schneider [52-53] observed when polystyrene solutions containing more than 2% polymer were irradiated in vacuo, the behavior of the system depended upon the solvent used. The viscosity of the solution either decreased steadily as in more dilute solutions, or increased with radiation dose until a gel was formed. Figure 3-2 is a plot of the limiting viscosity number of polystyrene irradiated in 5% solutions in various solvents. Of particular interest is the fact that in ethyl acetate, the viscosity of the solution increases with irradation and crosslinking occurs with a high efficiency.

The influence of polymer concentration was also studied by Henglein and Schneider [53]. The critical dose for incipient gel formation was determined in ethyl acetate solutions of polystyrene over a broad range of polymer concentrations. The results are summarized in Figure 3-3. The curve exhibits a pronounced minimum at about 20% concentration. Further, the shape of the plot of gel dose versus polymer concentration seems to be characteristic of crosslinking in polymer solutions in that very similar curves have been obtained in a number of other polymers [47].

Returning to the original problem of whether radiation induced crosslinking of the NE 102A scintillator solution is feasible, a comparison with the irradation of polystyrene solutions is now offered. The recipe cited in Chapter 2 yields a 20% NE 102A solution in a predominantly ethyl acetate solvent. Indeed, it is fortuitous that these conditions are optimum for crosslinking in polystyrene and

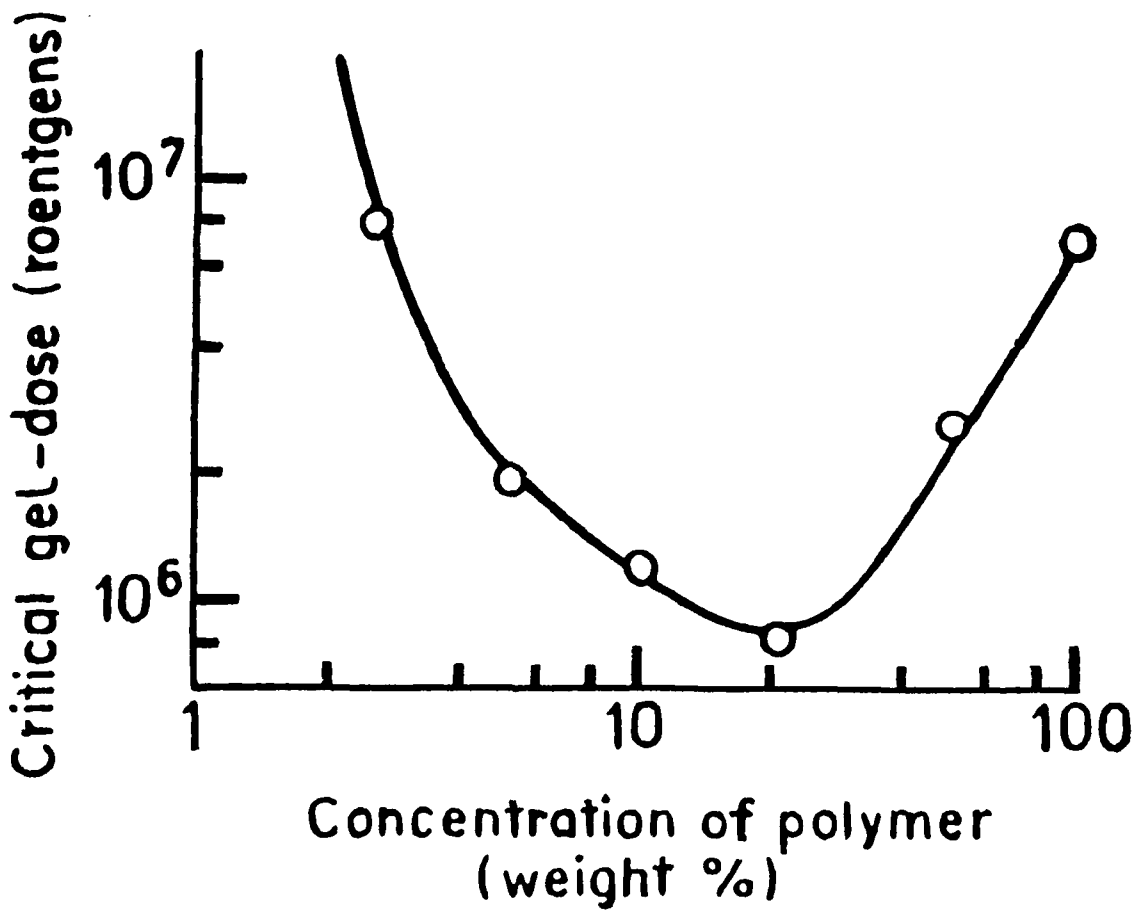

Figure 3-3 Influence of concentration of polystyrene in ethyl acetate solutions on the critical dose for incipient gel formation. Taken from ref. [43].

should be near optimum for crosslinking in PVT. In fact, Chernova et al. [54] have compared the radiolysis of polystyrene and polyvinyltoluene in solid phase and in solution, and reported the methyl group in the benzene ring actually enhances the efficiency of radiation crosslinking and prevents the degradation of the main chain.

The presence of small amounts of p-terphenyl and POPOP in the scintillator solution should pose no real problem. Aromatic systems behave as energy sinks or sponges and cause an increase in radiation resistance [41]. It is this protective action of the benzene ring in polystyrene which necessitates very large doses to produce any noticeable change. Even larger doses are expected for inducing crosslinks in the NE 102A scintillator solution.

Experimental

An NE 102A scintillator solution was prepared per the procedure detailed in Chapter 2. Approximately equal aliquots of scintillator solution were then placed in four glass test tubes (13 mm diameter) equipped with ground glass stoppers. The stoppers were seated snuggly and, as an additional precaution against escape of the volatile ester solvent, parafilm was wrapped tightly around the seal. These four samples were then used for conducting the crosslinking.

The irradiations were carried out at room temperature (~24°C) in a ^{60}Co gamma ray source [55]. The samples were irradiated for 0 hours (control), 8 hours, 16 hours, and 24 hours.

After exposure to the 1.173 MeV and 1.332 MeV gamma rays, the intrinsic viscosity was determined for each sample of scintillator solution. Viscosity measurements were made in cyclohexane solvent using a #75 Ubbelohde viscometer kept at 20.0°C by a constant temperature bath.

Thin films were also made from each of the samples (except the 24 hr sample) using the procedure described in Chapter 2. However, VYNS films were not used to sandwich the NE 102A laminations. Films could not be made from the sample irradiated for 24 hours because of the much increased viscosity of the scintillator solution at the gel point--the solution simply would not flow out over the water.

The response of the films was measured using ^{252}Cf fission fragments. The experimental configuration which was used to obtain TFD, SSD, TOF and timing resolution (RES) spectra is shown schematically in Figure 3-4. SSD and TOF spectra were obtained for each test TFD with it inserted and with it withdrawn; relative shifts of fission fragment pulse height peak positions to different channel numbers were used to estimate energy loss caused by the TFD. Calibration for the TOF and RES spectra were obtained by adding known lengths of cable to increase the delay on the stop signals sent to the time-to-amplitude converters. The timing calibration for the TOF spectra is shown in Figure 3-5 and the calibration curve for the RES timing is shown in Figure 3-6. Each spectrum was accumulated over a 4 hour period or approximately 10^5 events. Data acquisition and histogramming into 1K spectra were accomplished using a LeCroy 3500 computer.

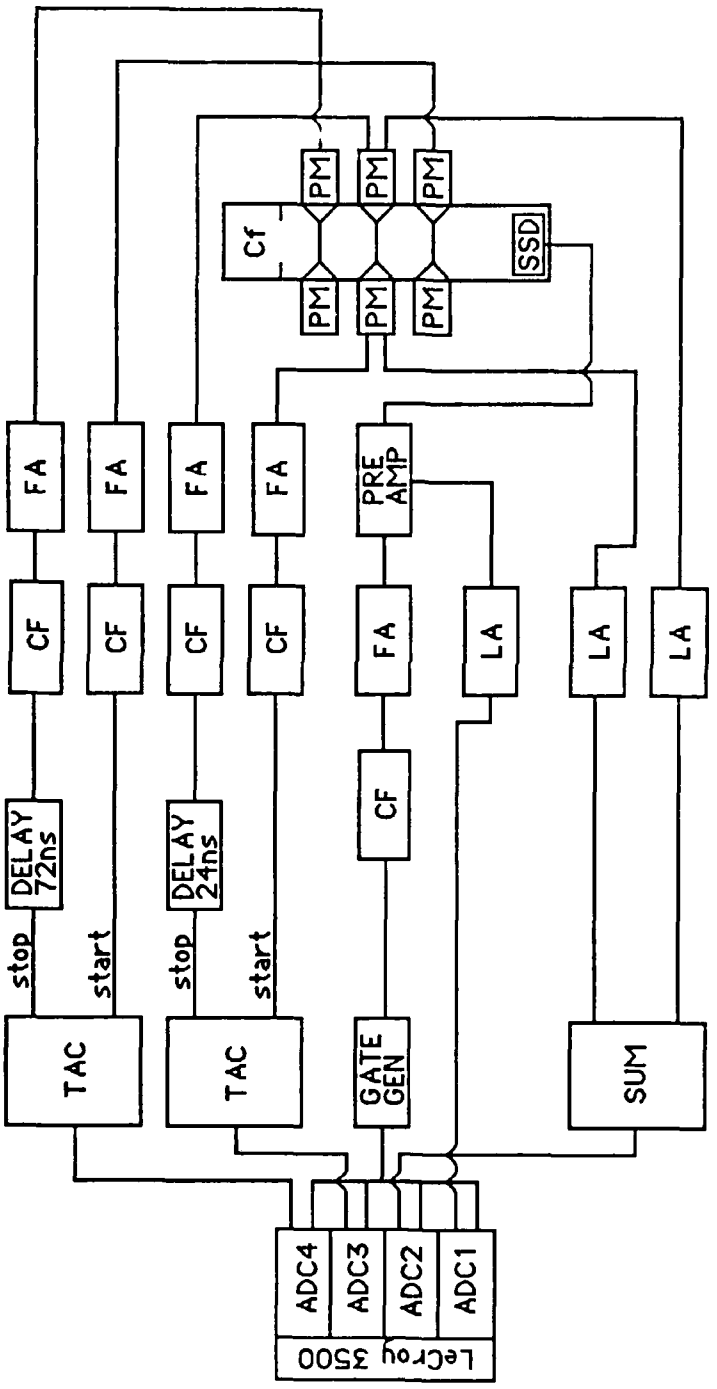

Figure 3-4 Schematic of experimental set-up used in this work for testing thin films.

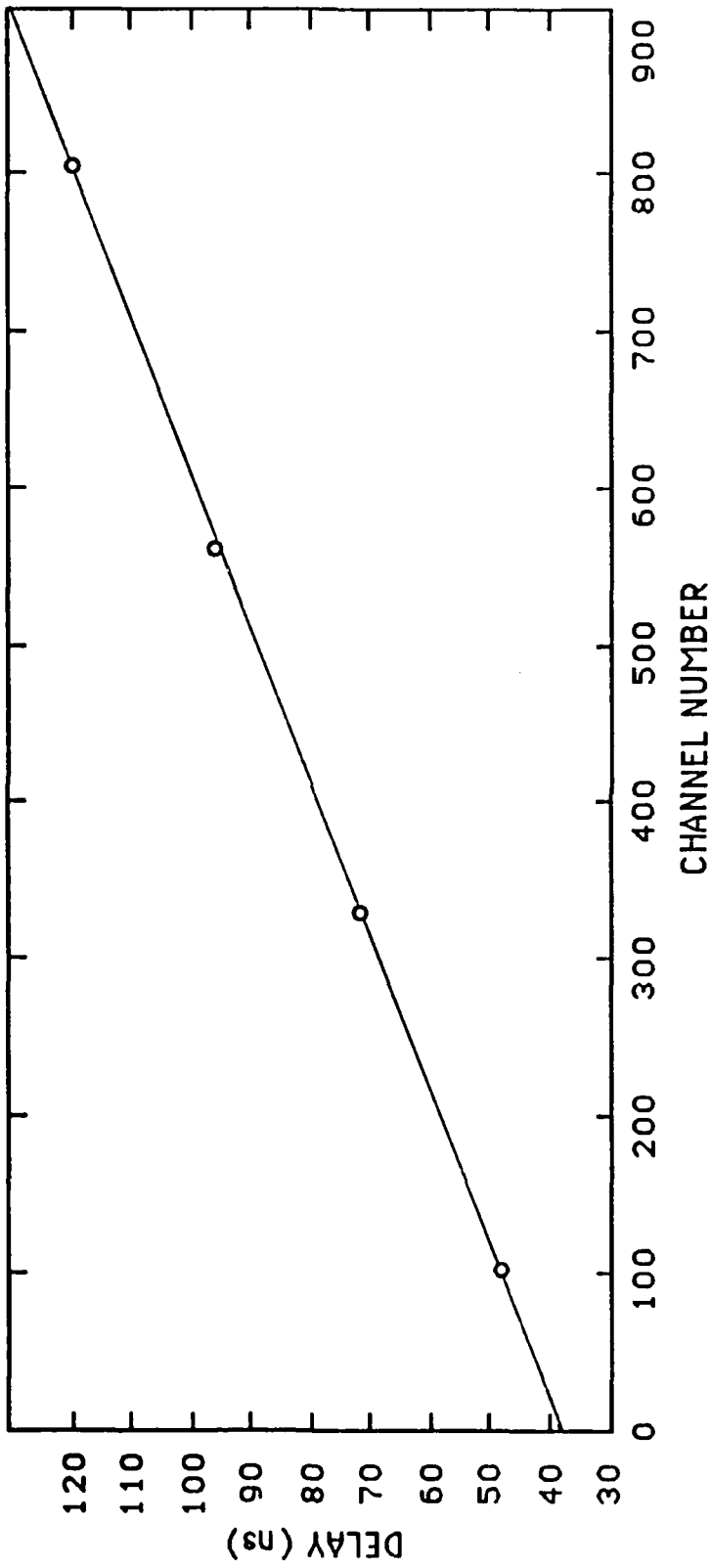

Figure 3-5 TOF calibration curve.

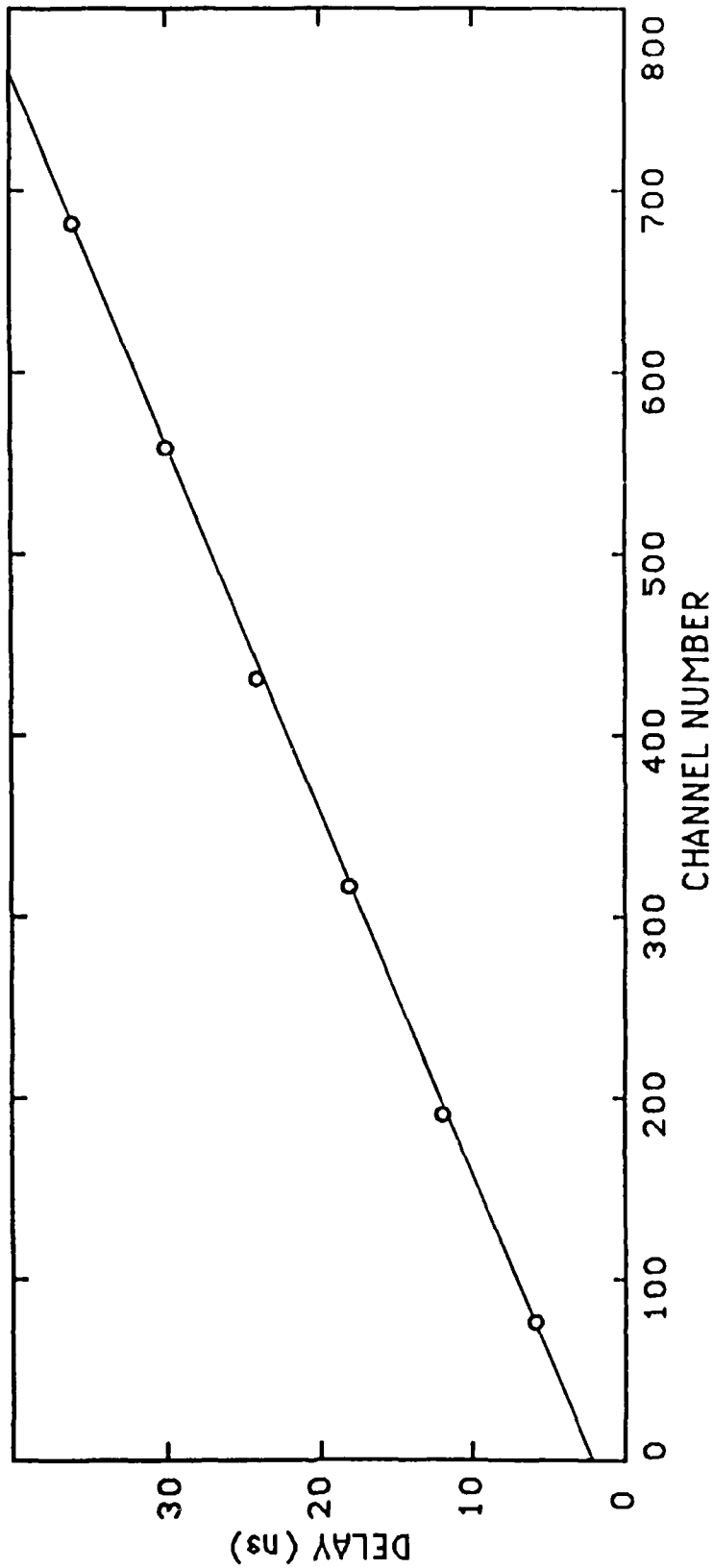

Figure 3-6 Timing resolution calibration curve.

The areal densities of the six films tested were obtained by weighing a section of film of known area on an analytical balance. Since this procedure destroys the films, weighing was conducted at the conclusion of testing.

Calculations

Dosimetry

The rate of energy input by the ^{60}Co source to the NE 102A scintillator solutions can be calculated by comparison to a chemical dosimeter. Gupta and Hanrahan [56] reported the dose rate to be 1.90×10^{19} eV $mL^{-1}hr^{-1}$ on August 1, 1985 based on Fricke dosimetry. The dosimeter solution was prepared per Weiss et al. [56] and the irradiations were carried out in 13 mm diameter glass test tubes with ground glass stoppers--the same type vessel used for irradiating the NE 102A solutions.

Using the exponential law for radioactive decay:

$$R = R_o e^{-\lambda t} \qquad \text{(Eq. 3-1)}$$

where:

R_o = initial dose rate

R = dose rate after t years

λ = decay constant

= 0.1315 yr^{-1} for ^{60}Co

t = time elapsed in years

the dose rate on July 20, 1987 (period when the NE 102A solutions were irradiated) was calculated to be 1.47×10^{19} eV $mL^{-1}hr^{-1}$ in Fricke solution.

The dose rate in the chemical dosimeter can be used to calculate the dose rate in the NE 102A solutions. Spinks and Woods [39] offer the following equation for the conversion of dose rates for different materials:

$$R_2 = R_1 \frac{(\overline{Z/A})_2}{(\overline{Z/A})_1} \text{ rads/hr} \qquad \text{(Eq. 3-2)}$$

where: R_1, R_2= dose rates in material 1 and material 2 respectively

$(\overline{Z/A})$= mean value of atomic number to atomic weight ratio.

The mean value of Z/A is calculated from

$$\overline{Z/A} = \Sigma\, w_i\, (Z/A)_i \qquad \text{(Eq. 3-3)}$$

with W_i being the weight fraction of the ith element in the medium.

The Fricke solution contained 0.002 M $Fe(NH_4)_2(SO_4)_2$ in 0.4 M H_2So_4 and thus applying Eq. 3-3, $\overline{Z/A}$ = 0.554. The scintillator solution contained 20% NE 102A, 76% $CH_3CO_2CH_2CH_3$ and 3% $CH_3CO_2(CH_2)_4CH_3$. The resulting $\overline{Z/A}$ = 0.545.

Finally, converting the dose rate in Fricke solution (d = 1.024 g/mL) from eV $mL^{-1}hr^{-1}$ to rad hr^{-1} and applying Eq. 3-2, the dose rate in the NE 102A solution is calculated to be 2.26×10^5 rads hr^{-1}. This is equivalent to 1.27×10^{19} eV $mL^{-1}hr^{-1}$ based on a scintillator solution density of 0.8989 g/mL.

Molecular Weight Determination

Many excellent works have been written adressing the behavior of polymers in solution and methods for estimating their average molecular weight [41-44,58-62]. The intrinsic viscosity of polymer solutions is traditionally used in polymer chemistry for determining molecular weights of macromolecules. The viscosity average molecular weight, $\bar{M}_v$, and the intrinsic viscosity, $[\eta]$, are related through the Mark-Houwink-Sakurada equation:

$$[\eta] = K\bar{M}_v^{\,a} \qquad \text{(Eq. 3-4)}$$

where K and a are constants characteristic of a polymer-solvent pair at a given temperature. For PVT in cyclohexane at 20.0°C, K = 2.2 x 10^{-2} mL/g and a = 0.68 [63,64]. However, it should be noted that [n] is a measure of the hydrodynamic volume of the polymer molecule and is, therefore, greatly affected by the geometric configuration of the polymer. Thus, for a given molecular weight, the viscosity is strongly dependent upon the extent of branching in the polymer.

Since crosslinking necessarily proceeds via chain branching, it is risky to base molecular weights of irradiated polymers on intrinsic viscosity measurements alone, unless it is known that no crosslinking occurs. Shultz et al. [61] studied this particular problem and derived the expected change of viscosity as a function of radiation dose. The results are expressed as a function of the ratio of the actual radiation dose D to the cricial radiation dose D* required for incipient gel formation, the ratio of the probabilities

of main chain scission to crosslinking, β/α, and the Mark-Houwink-Sakurada exponent, a. The theoretical curves for a = 0.70 are shown in Figure 3-7 along with the observed values for the NE 102A samples. The agreement between the experimental curve and the theoretical curve for $\beta/\alpha = 0$ is rather good and confirms the earlier prediction that irradiation of the NE 102A solutions would result in crosslinking only, with essentially no scission.

The intrinsic viscosities were determined experimentally for the three pre-gel scintillation solutions by measuring the flow times for varying dilutions in cyclohexane and employing the following relationship:

$$[\eta] = (\eta_{red})_{c=0} \qquad \text{(Eq. 3-5)}$$

where the reduced viscosity, η_{red}, can be defined as:

$$\eta_{red} = \frac{t - t_o}{t_o C} \qquad \text{(Eq. 3-6)}$$

for t, t_o > 100 s. In this relationship, t_o is the flow time for the pure solvent and t is the flow time for the diluted polymer at concentration, C, given in g/mL.

The viscometric parameters for the 0 hr, 8 hr, and 16 hr irradiated solutions are given in Table 3-1. A plot of η_{red} versus C for each sample is shown in Figure 3-8; each line was regressed using a least squares best fit with the value of $[\eta]$ determined by the y-intercept.

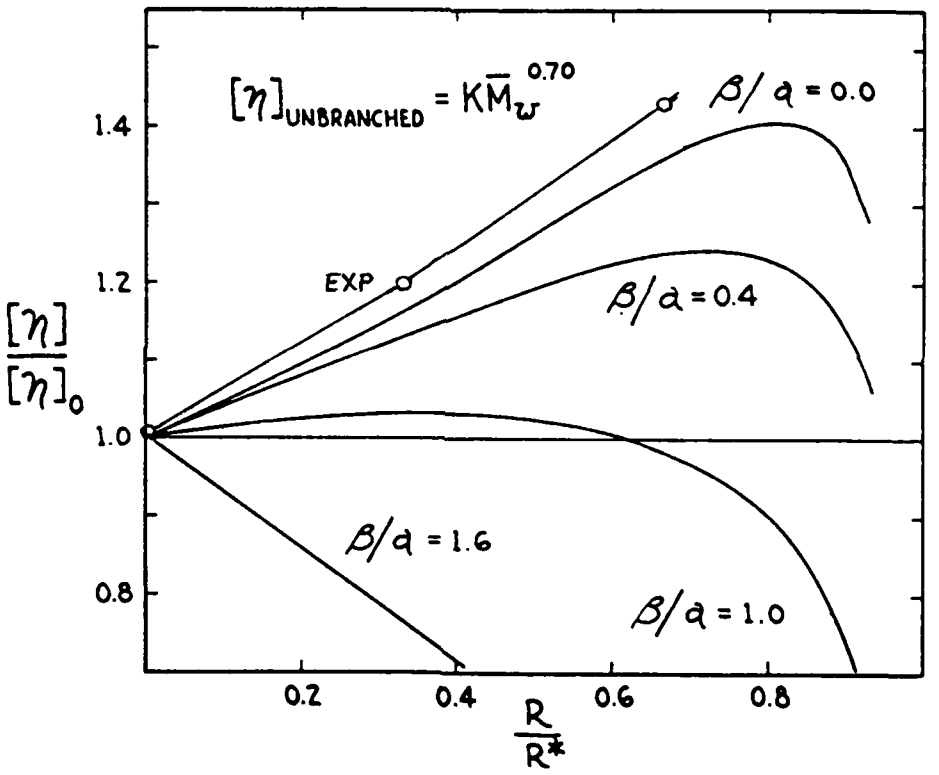

Figure 3-7 Theoretical ratio of irradiated to non-irradiated polymer intrinsic viscosities plotted gainst fraction of gelling dose for chosen values of β/α. The Mark-Houwink-Sakurada exponent is a = 0.70. Observed ratios for irradiated NE 102 solutions are also shown. Adapted from ref. [61].

Table 3-1 Viscometric Parameters

Sample Irradiation Time (hours)	$C \cdot 10^4$ (g/mL)	t (s)	η_{red} (mL/g)	$[\eta]$ (mL/g)	$[\eta]/[\eta_o]$
0	0	154.1		62.91	1.00
	6.101	160.1	63.82		
	9.151	163.2	64.53		
	10.98	165.3	66.19		
	0	154.1			
	12.20	166.4	65.42		
	18.30	172.9	66.67		
	21.96	176.9	67.38		
8	0	153.7		75.32	1.20
	6.141	160.9	76.28		
	9.211	166.0	86.88		
	1.105	168.9	89.50		
	0	154.8			
	12.28	171.0	85.22		
	18.42	180.4	89.78		
16	0	154.4		92.28	1.47
	6.209	163.9	99.10		
	9.314	169.0	101.5		
	11.18	172.2	103.4		
	0	155.1			
	6.209	164.4	97.09		
	9.314	169.6	100.7		
	11.18	172.8	102.1		

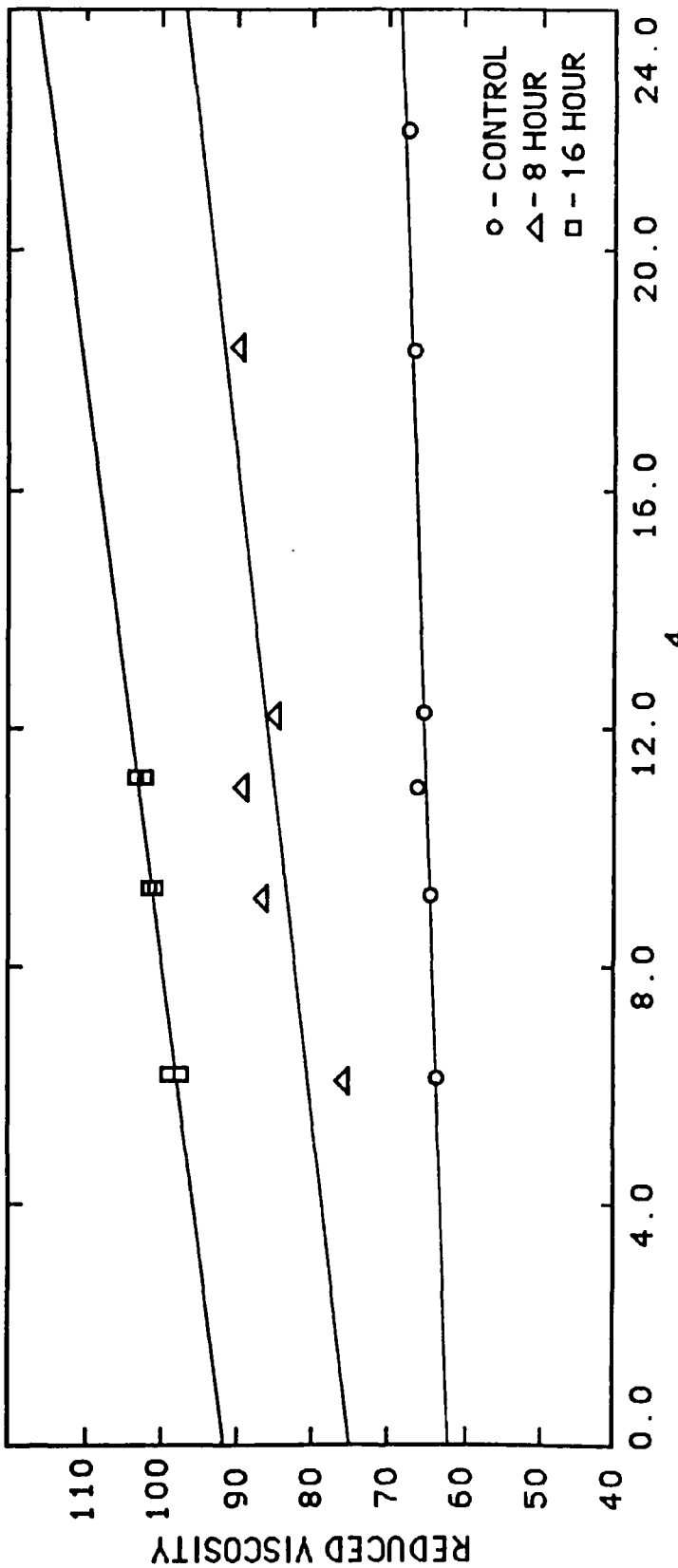

Figure 3-8 Reduced viscosity as a function of polymer concentration.

Charlesby [62] derived a relationship which enables the calculation of the weight average molecular weight for a given degree of crosslinking (up to the gel point) if the initial molecular weight is known. The expression is:

$$\frac{\bar{M}_w}{\bar{M}_{wo}} = \frac{1}{1 - \delta} \qquad \text{(Eq. 3-7)}$$

where $\bar{M}_{wo}$ is the initial weight average molecular weight of the polymer before irradiation, $\bar{M}_w$ is the weight average molecular weight of the polymer after receiving a given dose, and the crosslinking coefficient, δ, is simply the ratio of the absorbed dose to the dose needed for incipient gel formation. Figure 3-9 is a plot of $\bar{M}_w/\bar{M}_{wo}$ versus δ and the dose in rads based on the experimentally determined gelling dose of 5.42 Mrad (24 hr irradiation) for the NE 102A solution.

The Mark-Houwink-Sakurada equation can be used to calculate the initial molecular weight of the PVT polymer since no crosslinking (and subsequent branching) has been induced. Applying Eq. 3-4 to the 0 hr sample yields a viscosity average molecular weight of 121,000. Since $\bar{M}_v$ closely approximates $\bar{M}_w$ [44], the average PVT molecular weight can be estimated for any pre-gel dose. This correlation is also shown in Figure 3-9.

G Value

If it is assumed that random crosslinking between molecules is the only process occurring, then the gel point occurs when there is

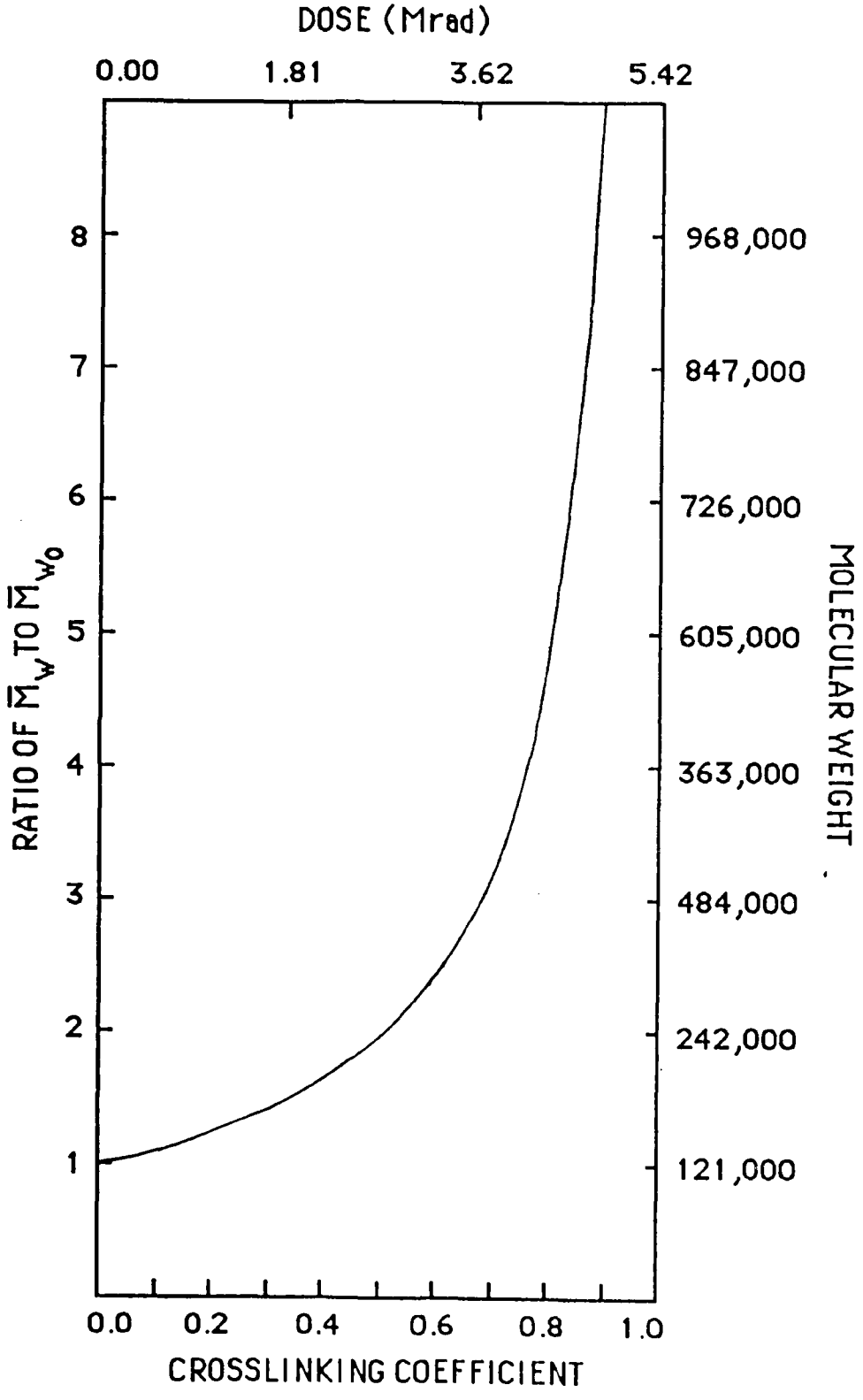

Figure 3-9 Increase in weight average molecular weight of PVT as a function of dose (and δ).

one monomer unit crosslinked per weight-average molecule originally present [40]. Since two monomer units must be joined to form one crosslink, the number of crosslinks formed per 100 eV absorbed, G, is given by:

$$G = \frac{100(6.023 \times 10^{23}\ \text{mole}^{-1})}{2(6.24 \times 10^{13}\ \text{eV rad}^{-1}\ \text{g}^{-1})\ M_w\ D^*} \qquad \text{(Eq. 3-8)}$$

Applying Eq. 3-8, G(crosslink) = 0.74 for NE 102A scintillator solution exposed to ^{60}Co gamma rays.

Spectral Parameters

Central channel number. The central channel numbers for the SSD and TOF spectra were found per the method described by Schmitt et al. [65]. The central channel number was obtained for both the heavy mass, M_H, and light mass, M_L, fragment peaks by determining the midpoint between the 3/4-maximum points. This method is illustrated in Figures 3-10 and 3-11 for SSD and TOF spectra obtained with the test TFD withdrawn out of the path of the fission fragments. The central channel numbers for each of the six thin films tested are tabulated in Table 3-2.

The observed shift in SSD central channel numbers when a TFD was inserted was used to estimate directly the energy degradation of the M_H and M_L fission fragments caused by the scintillator foil; the relative shift, given in channel numbers, divided by the initial (film withdrawn) channel number yields the percent energy degradation.

TABLE 3-2 Spectral Parameters

TFD	SSD CENTRAL CHANNEL NOs.				INVERSE TOF CENTRAL CHANNEL NOs.				TIMING RESOLUTION FWHM (CHANNELS)
	FILM WITHDRAWN		FILM INSERTED		FILM WITHDRAWN		FILM INSERTED		
	M_H	M_L	M_H	M_L	M_H	M_L	M_H	M_L	
A	355	530	227	380	357	398	339	389	10.4
B	356+	530+	148	266	358+	398+	324	380	10.4
C	344*	510*	206*	349*	358	399	332	386	10.8
D	361	537	306	475	358	398	352	396	16.8
E	355	528	108	202	358	399	305	367	9.6
F	351	523	285	453	357	398	349	394	12.8

+ Value determined by averaging the channel numbers obtained for films A, D, E, and F.
* SSD spectra had very poor resolution; an instabilty in the electronics is suspected.

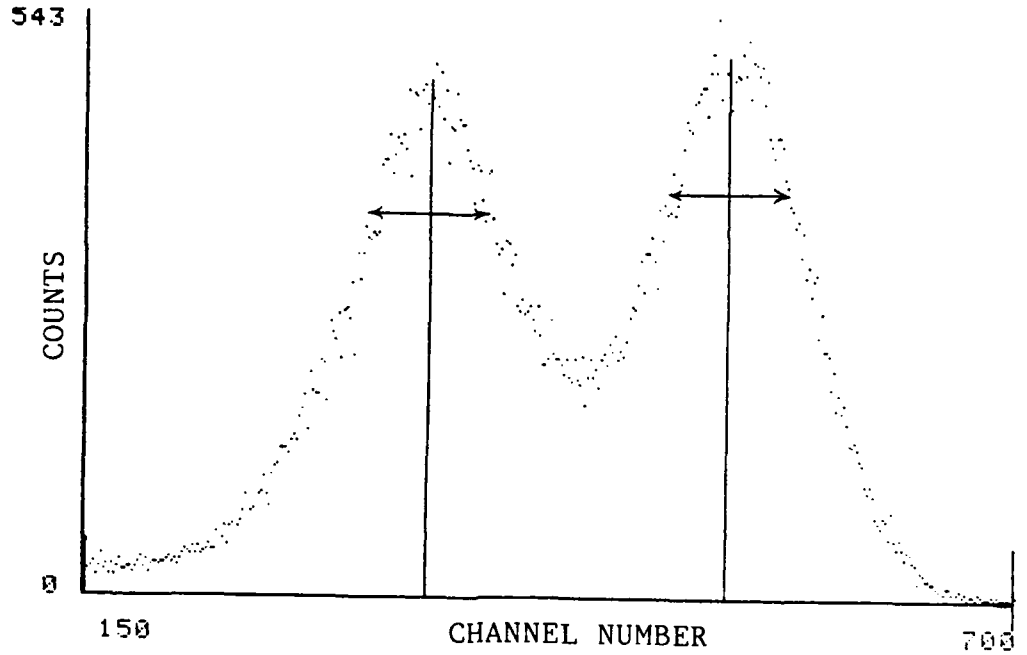

Figure 3-10 Calculation of SSD central channel numbers. SSD spectrum is with film withdrawn.

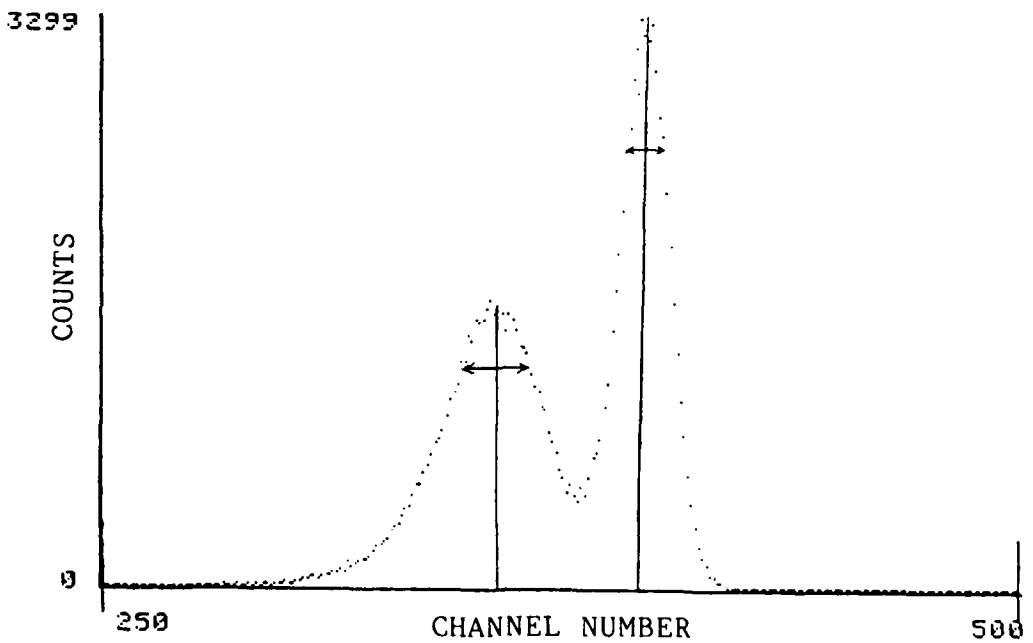

Figure 3-11 Calculation of TOF central channel numbers. TOF spectrum is with film withdrawn.

The shift in TOF central channel numbers was related directly to the increased TOF due to fission fragment velocity attenuation upon passing through the test TFD. Since the first and third scintillator films in the experimental arrangement (see Figure 3-4) were not changed through the course of the experiment, any increase in flight time must be due to the second or test thin film. The relative shift for both M_H and M_L TOF peaks, expressed in channel numbers, was converted to time using the slope of the TOF calibration curve shown in Figure 3-5.

Full-width-half-maximum (fwhm). The timing resolution for each TFD was calculated at fwhm. The fwhm value was determined by counting the number of channels between the half-maximum points of the RES spectrum. The fwhm resolution expressed in channel numbers is given for each TFD in Table 3-2. The width in channel numbers was converted directly to units of time using the slope of the RES calibration curve shown in Figure 3-6. The RES spectra obtained for all of the thin films are presented in Figures 3-13,15,17,19,21, and 23.

Peak-to-valley ratio (P/V). In order to quantitatively compare thin films, the P/V was determined for each TFD spectrum (Figures 3-12,14,16,18,20, and 22). The P/V was defined as the ratio of the left hand (M_H) peak height to the height of the valley above the base line. Table 3-3 summarizes the pertinent characteristics of each of the thin films.

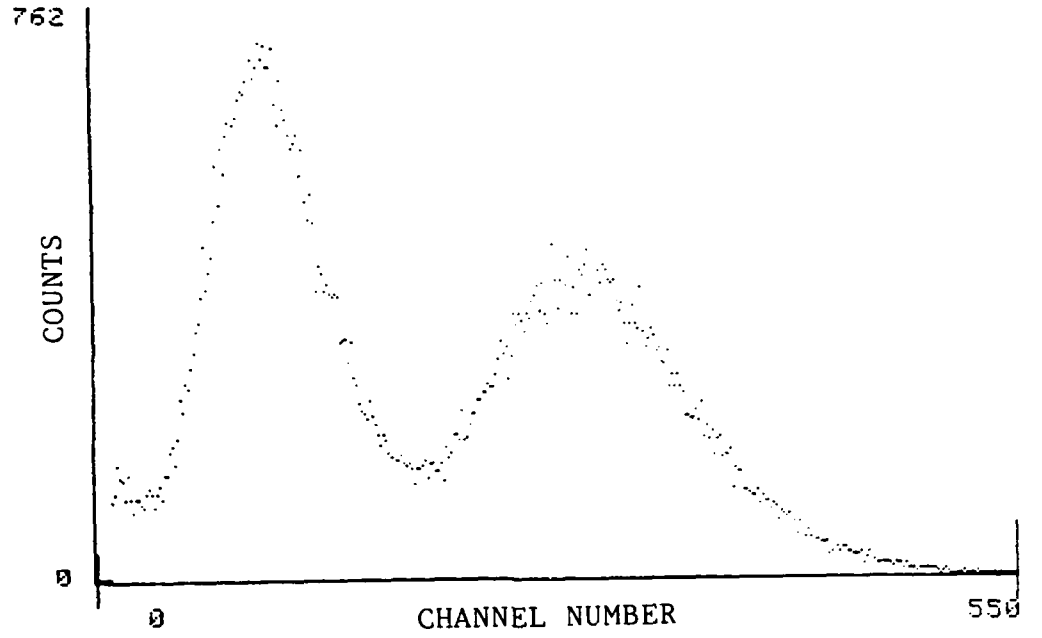

Figure 3-12 TFD A response.

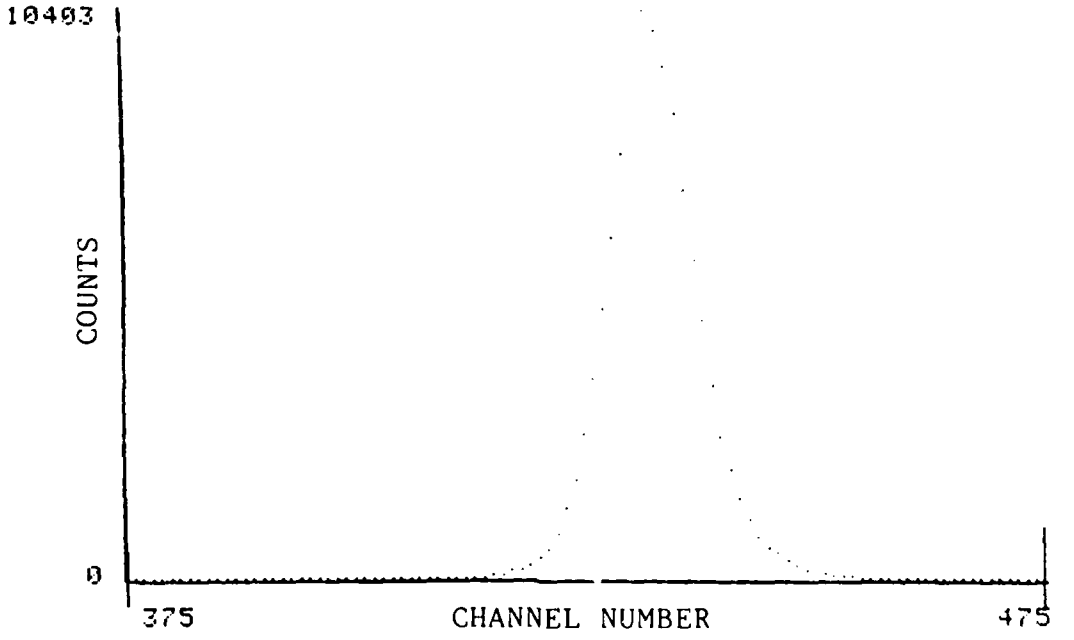

Figure 3-13 TFD A timing resolution.

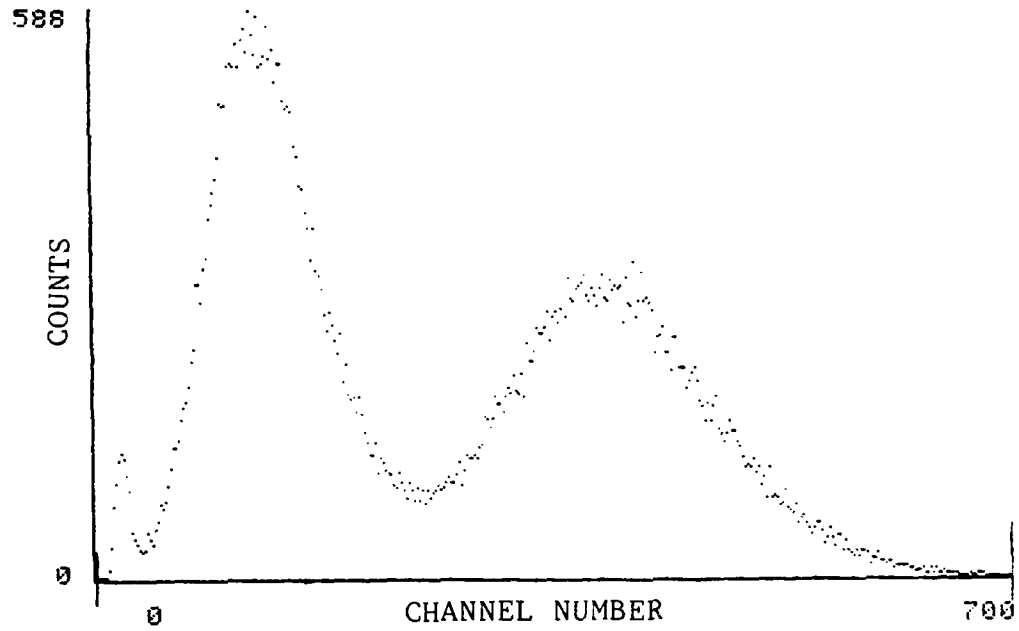

Figure 3-14 TFD B response.

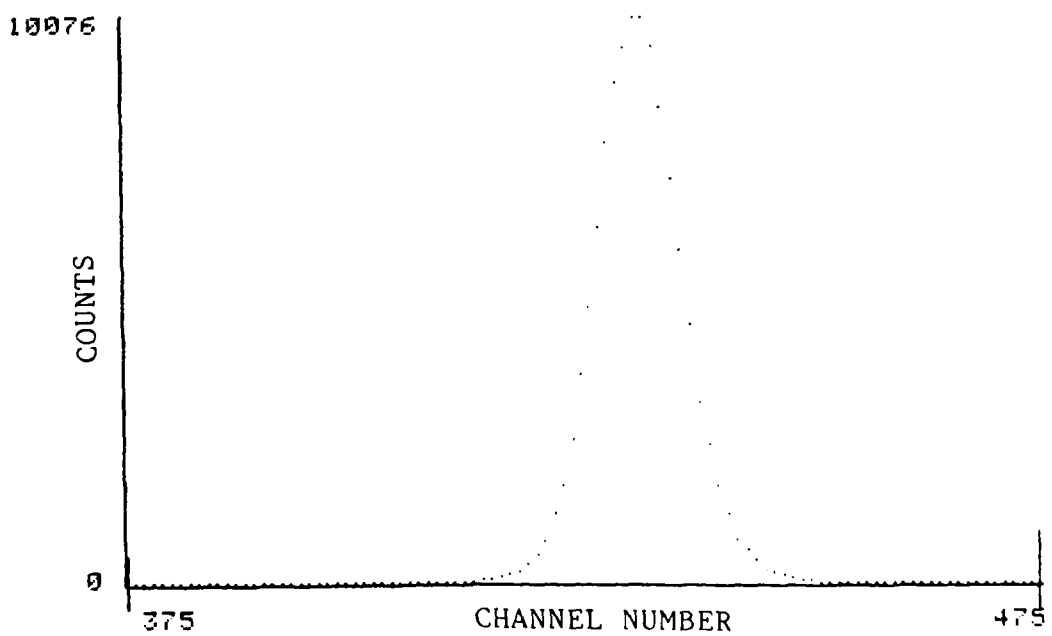

Figure 3-15 TFD B timing resolution.

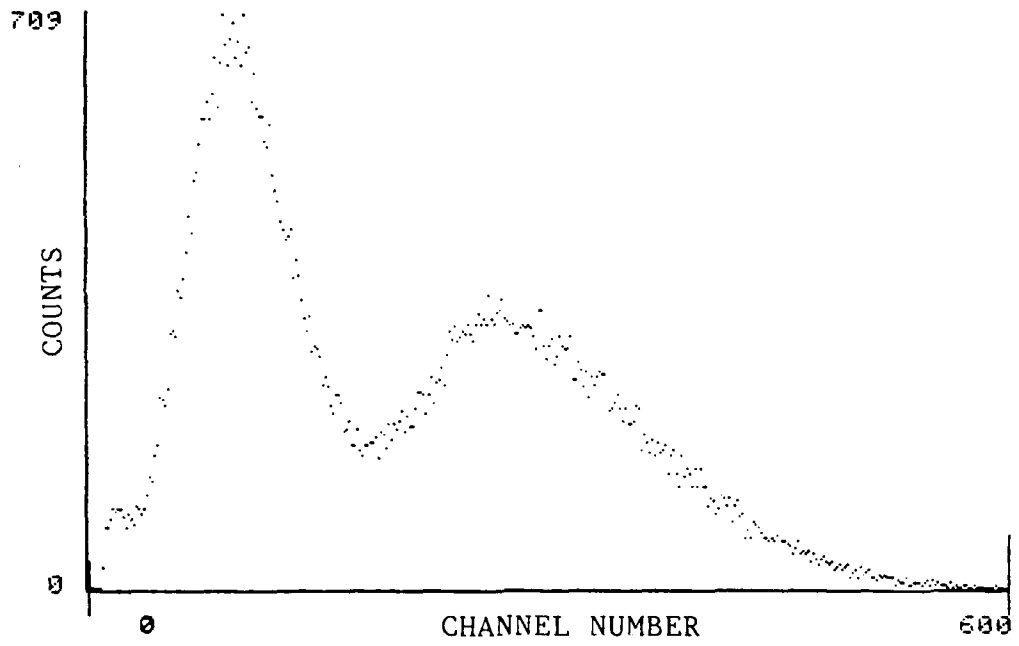

Figure 3-16 TFD C response.

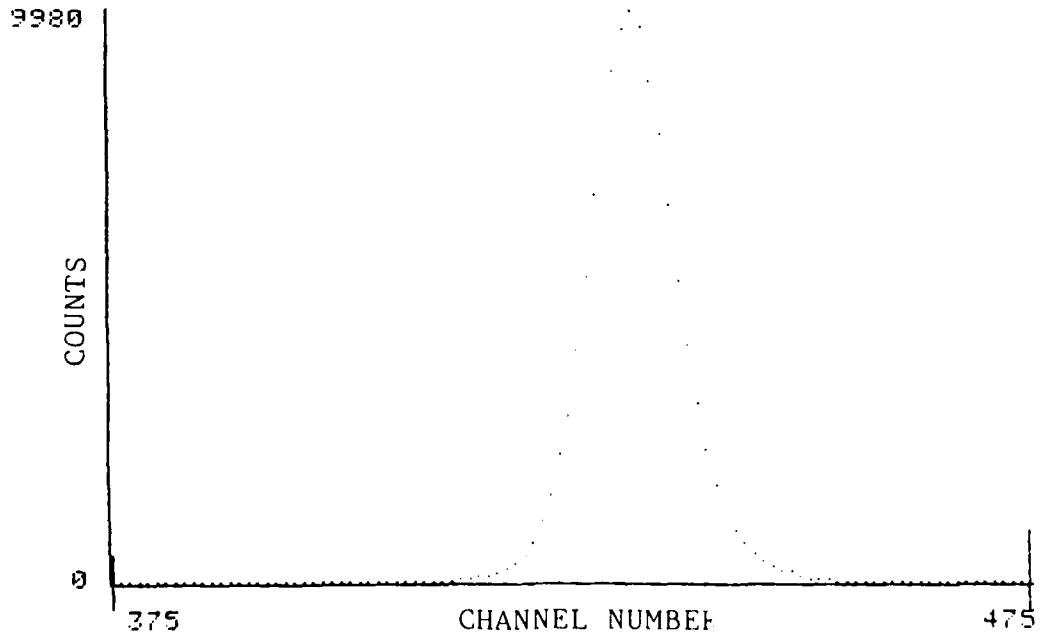

Figure 3-17 TFD C timing resolution.

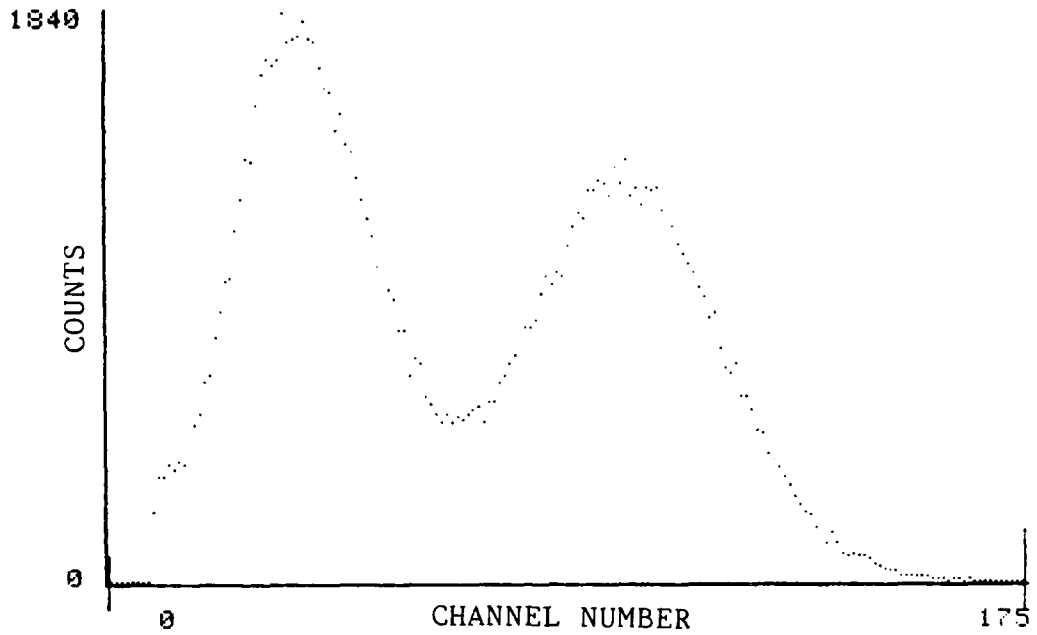

Figure 3-18 TFD D response.

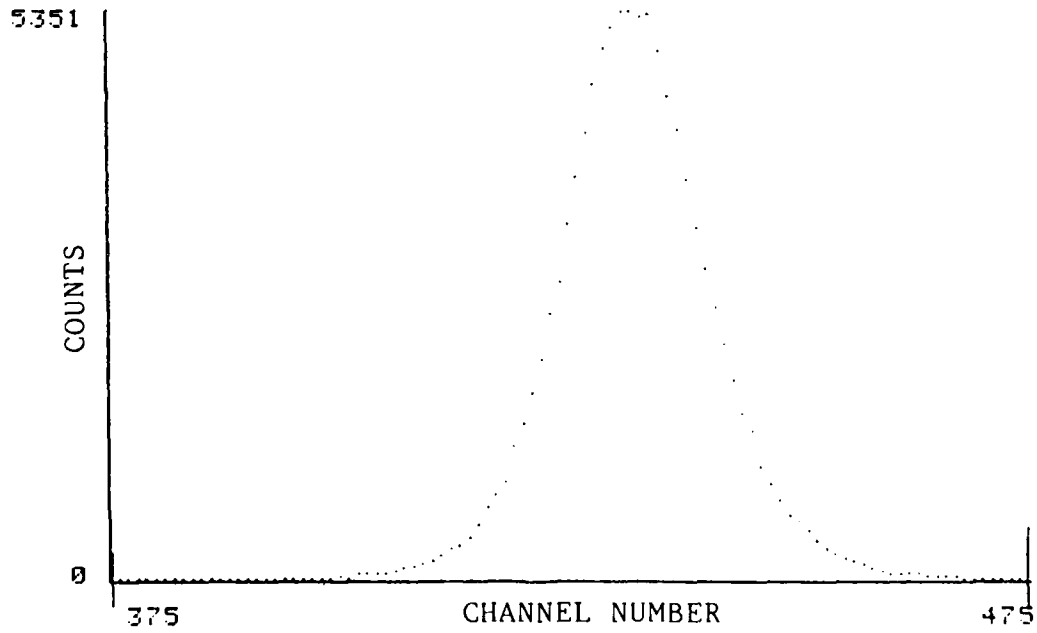

Figure 3-19 TFD D timing resolution.

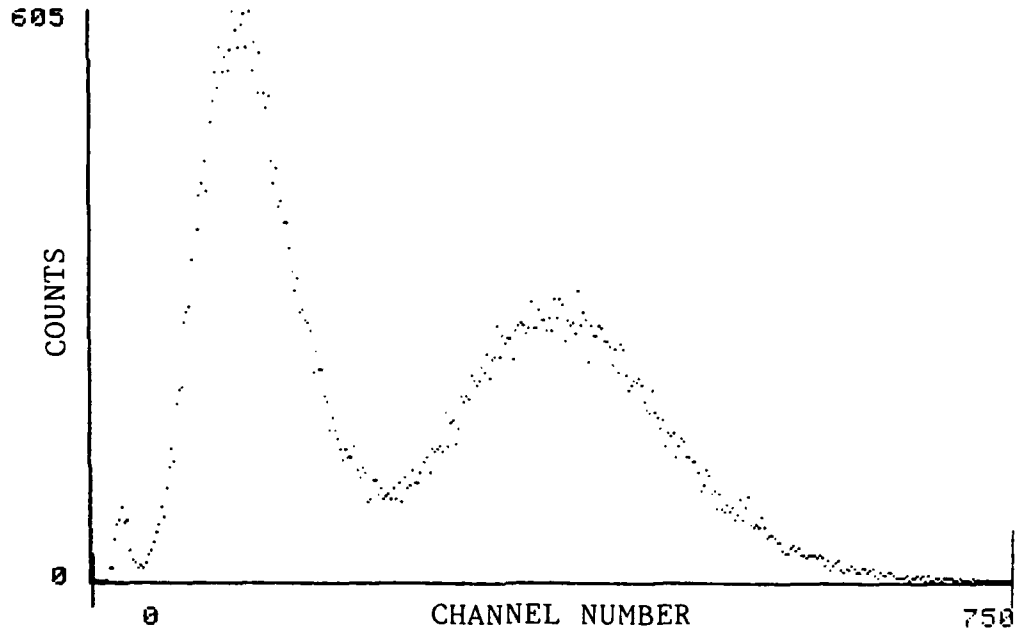

Figure 3-20 TFD E response.

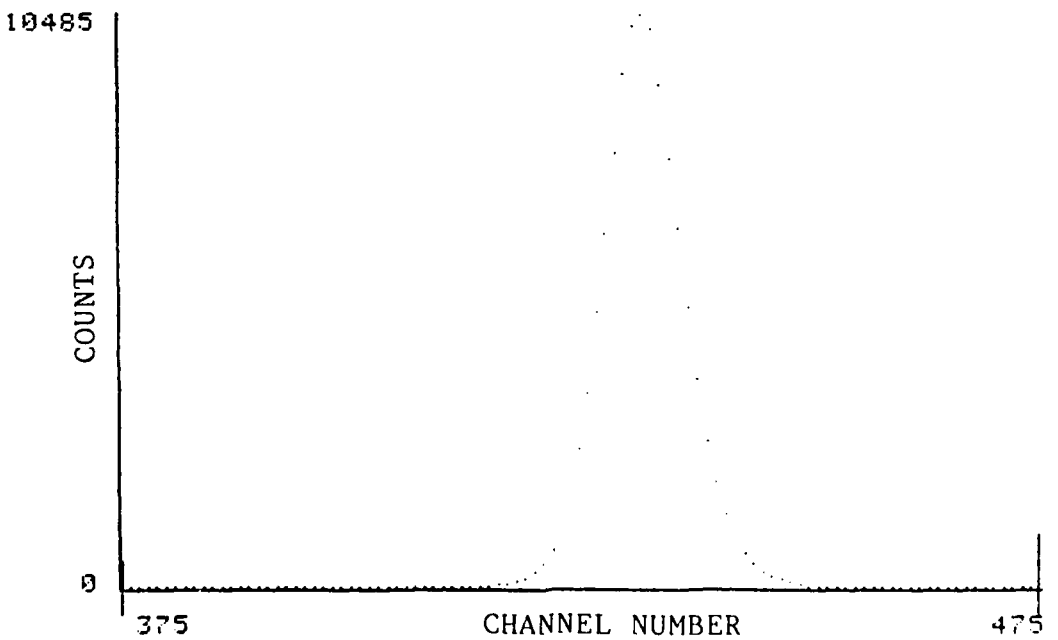

Figure 3-21 TFD E timing resolution.

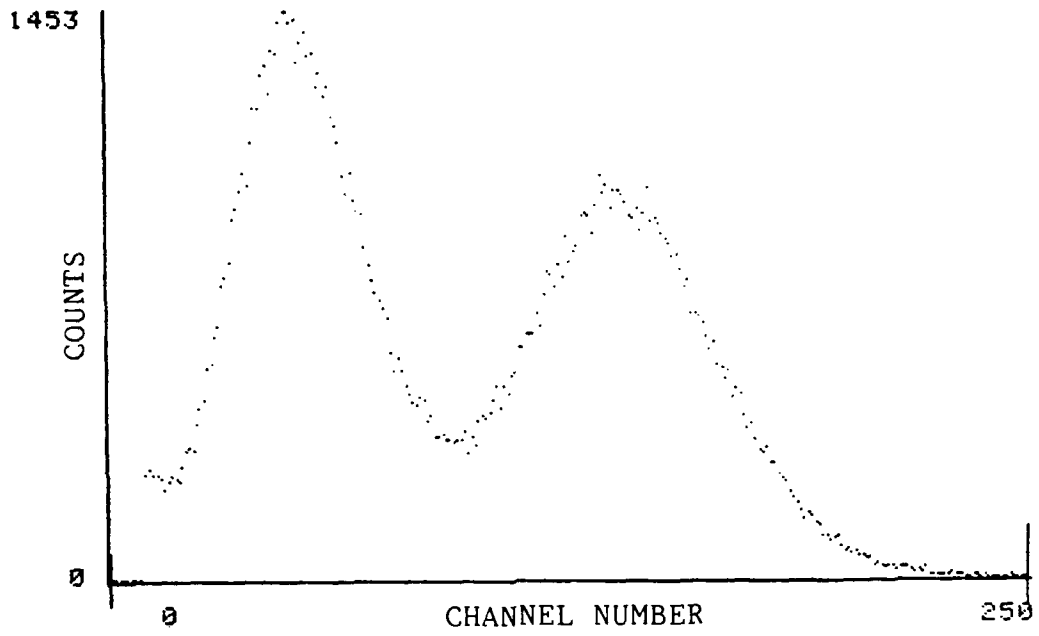

Figure 3-22 TFD F response.

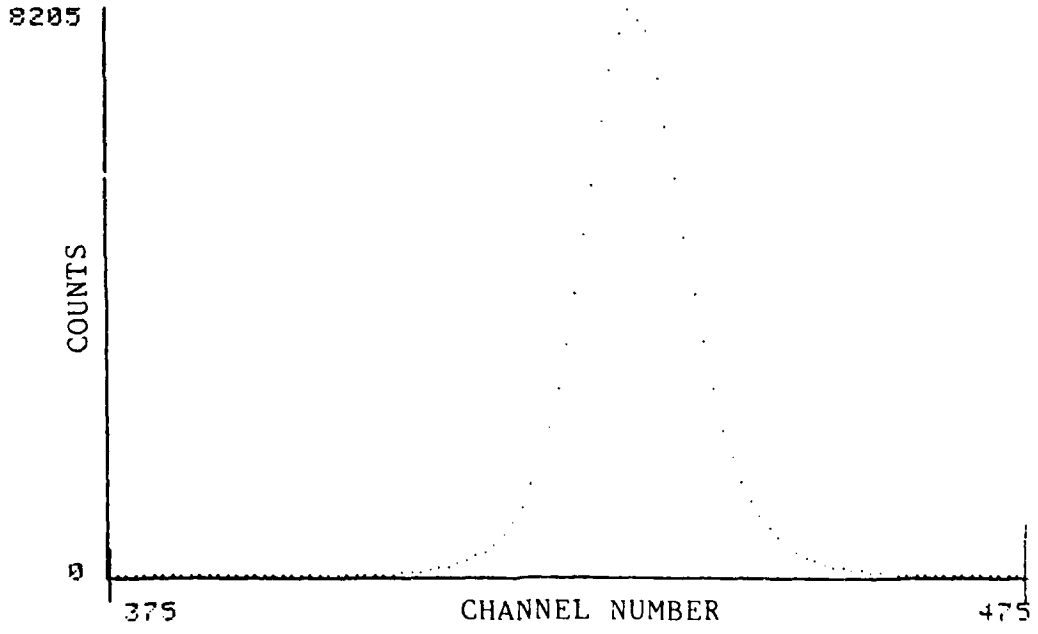

Figure 3-23 TFD F timing resolution.

TABLE 3-3 TFD Characteristics

TFD	Dose (Mrad)	$\bar{M}_w$ of PVT	No. of Lamina-tions	Film Thickness ($\mu g/cm^2$)	ENERGY LOSS(%) M_H	M_L	TOF INCREASE (ns) M_H	ML	TIMING RESOLUTION FWHM (ps)	P/V
A	0	121,000	4	260	36.1	28.3	1.861	0.931	514	5.2
B	0	121,000	3	470	58.4	49.8	3.516	1.861	514	6.7
C	1.81	182,000	3	440	40.1	31.6	2.688	1.344	533	4.2
D	1.81	182,000	2	70	15.2	11.5	0.620	0.207	830	3.5
E	3.62	363,000	2	630	69.6	61.7	5.480	3.309	474	6.5
F	3.62	363,000	1	140	18.8	13.4	0.827	0.414	632	4.2

+ E_L (MeV) = 104.4 ± 1.0; E_H (MeV) = 78.3 ± 0.7 for non-degraded ^{252}Cf fission fragments [66].

Results and Discussion

Since the six thin films tested were unfortunately all a different thickness, direct comparison between films is not possible. Nevertheless, because each pair of films made from the three pre-gel solutions brackets a rather large interval, and considerable overlap exists between the three pairs of films, it is possible to analyze the effect of crosslinking on thin film response.

The energy degradation for both M_H and M_L fragments as a function of film thickness is plotted in Figure 3-24. Of particular significance is the fact that the M_H points define a line with correlation greater than 0.99 and the M_L points also define a line with correlation exceeding 0.99; the set of data points obtained for Film C were not included in the regression because the spectra are suspect; the SSD spectra for Film C were very poorly resolved and an electronic malfunction is suspected. Since all four parameters measured for each thin film were gated with the SSD signal, all data points for Film C are unreliable. They are shown in brackets in Figure 3-24 and subsequent figures, but are not included in linear regression analyses. Even so, the excellent linearity between the other data points suggests the energy loss of fission fragments is a smooth function of film thickness over the range studied (0 - 630 $\mu g/cm^2$), and that crosslinking of the PVT matrix has no detectable effect on the stopping power of the films. The essentially linear dependence of energy loss on film thickness is certainly expected in terms of the Bragg curve for positive heavy ions [37]. The greater energy loss experienced by the heavy fragments at a given film

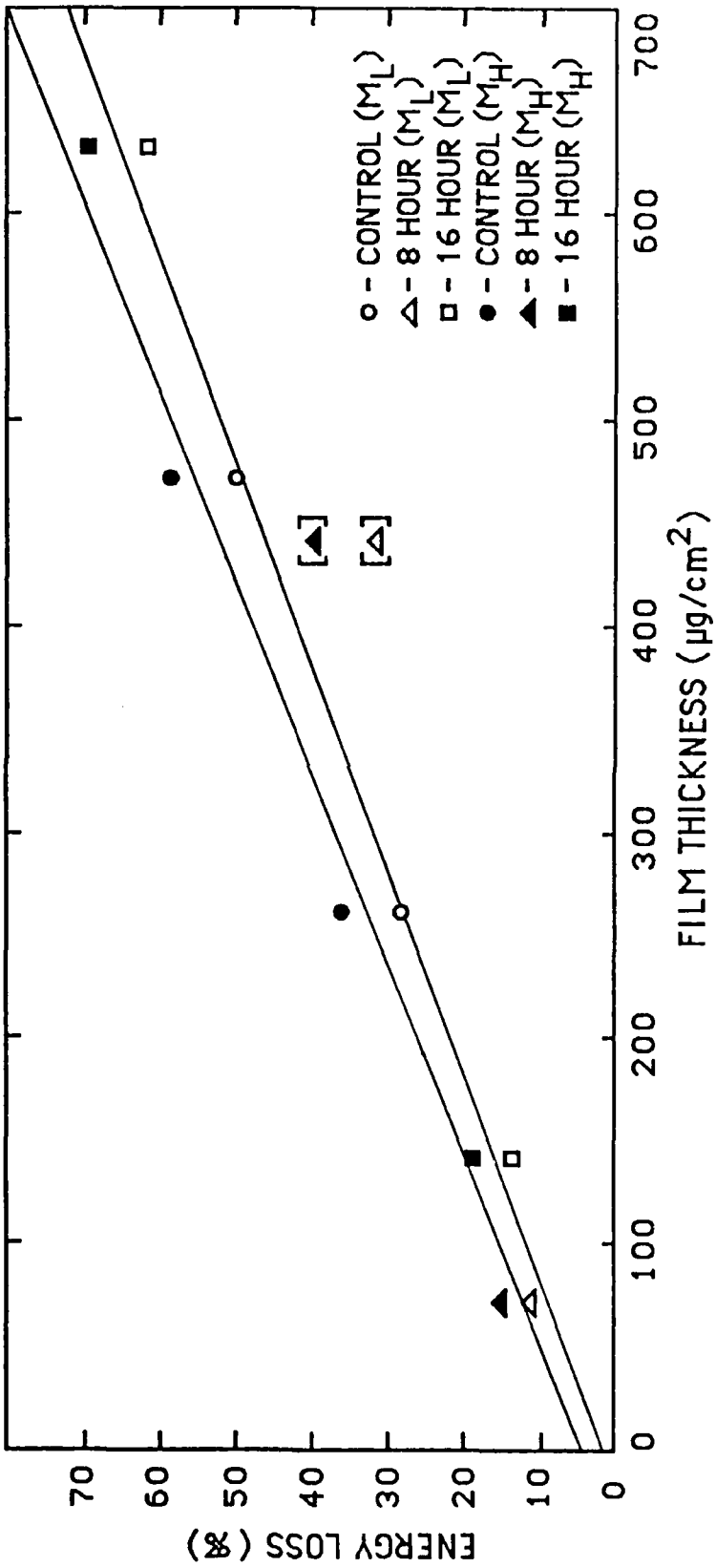

Figure 3-24 Fission fragment energy loss as a function of film thickness.

thickness is expected since they carry higher effective charges, and are travelling at lower velocities than the light fragments.

Figure 3-25 shows the increase in flight time (velocity attenuation) for fission fragments as a function of film thickness. Again two well-defined lines emerge (corr. > 0.99 for M_H and corr. > 0.98 for M_L) further suggesting the stopping power of the films was unaffected by the radiation induced crosslinking.

Perhaps the most revealing analysis is shown in Figure 3-26 which is a plot of P/V versus thin film thickness. An approximately linear relationship is observed (corr. > 0.94) with no obvious distinction in TFD response attributable to the degree of crosslinking.

The results clearly show the behavior of thin films made from crosslinked NE 102A solutions is indistinguishable from those made from the non-crosslinked control solution. Apparently the scintillator solution undergoes little if any degradation for doses up to 3.62 Mrad as discussed earlier in this chapter, and energy transfer processes from solvent to fluor are unaffected by the increases in PVT molecular weight and attendant branching.

The original objective for conducting this study was to improve the strength of the NE 102A thin films without degrading their luminescent capabilities. Based on this criterion, the gamma ray induced crosslinking of the PVT matrix was unquestionably a success; the films made from the irradiated solutions were substantially stronger than the films made from the control solution. In fact, films made from the 16 hr (3.62 Mrad) solution were so strong that on several occasion they were lifted off the surface of the water with

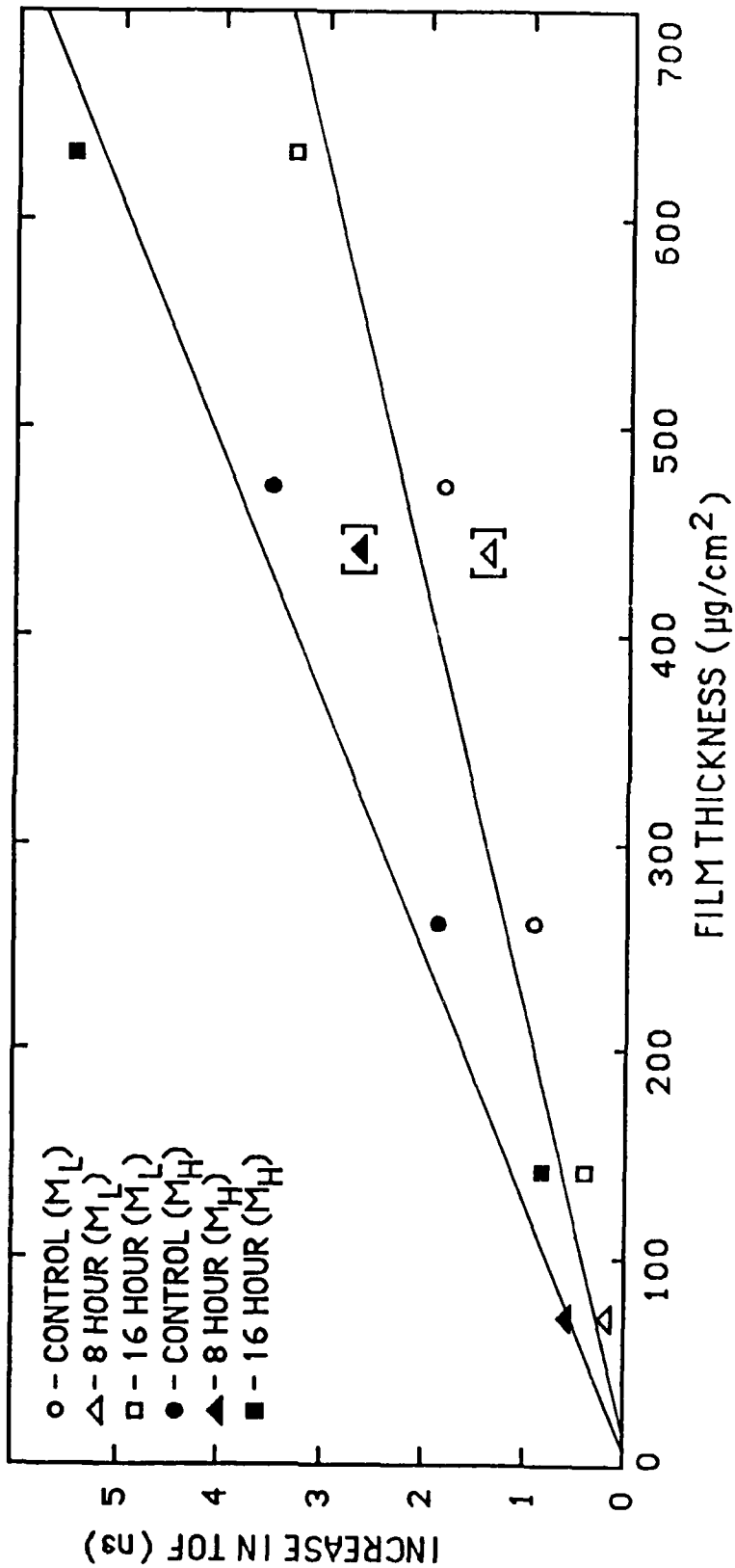

Figure 3-25 Increase in fragment flight time as a function of film thickness.

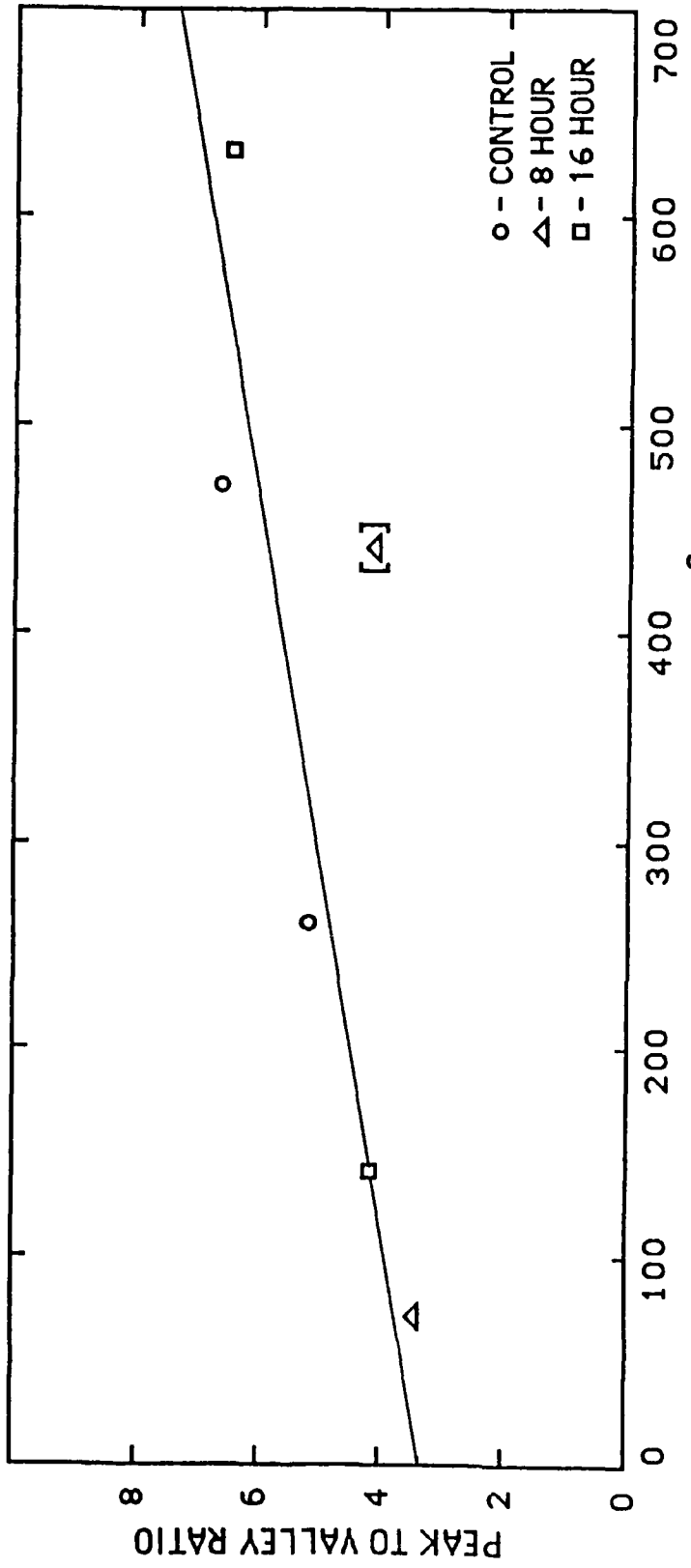

Figure 3-26 Peak-to-valley ratio as a function of film thickness.

bare hands and flattened out on top of the celluloid frame without causing a single tear or crack. Films made from the crosslinked solutions were typically thicker as well, though large variations in thickness between films made from the same solution were still evident.

In general, improved strength was observed with increasing degrees of crosslinking--yet without adverse effects of the scintillation properties. Additionally, crosslinked films offer a convenient way of obtaining thicker films with fewer laminations and tend to be extremely clear with singularly few blemishes.

CHAPTER 4
A PROTOTYPE BaF_2 THIN FILM

Introduction

Barium fluoride has been shown recently by Laval et al. [67] to have an intense fast component due to emission at 220 nm wavelength associated with the 310 nm wavelength band slow component. The fast component is characterized by a decay time constant equal to 600 ps and by a fwhm equal to 550 ps. BaF_2 crystals were shown to have a high time resolution equal to 112 ps for ^{60}Co gamma rays which was equivalent to that measured with NE 111, one of the fastest plastic scintillators (see Table 1-1). The total light output was approximately 20% that of NaI(Tl) crystals.

The excellent timing properties and good light yield are desirable properties for a potential thin film scintillator. However, since BaF_2 is a rather insoluble inorganic salt, a different method had to be devised to fabricate a thin film.

Experimental

The BaF_2 thin film was prepared by sedimentation from an aqueous slurry. This is an often used method for preparing targets when uniformity criteria are not too stringent [37]. Though extremely uniform thin films are required for good TFD spectra, films made

using the sedimentation technique should still prove useful in testing the concept validity.

The thin film was fabricated by placing several drops of a BaF_2/H_2O slurry on the surface of a previously mounted VYNS film. The slurry was spread evenly over the surface of the VYNS and the water allowed to evaporate at room temperature and atmospheric pressure. The assembly was partially covered with a large flask to reduce the settling of dust on the film. After the water had evaporated completely (3 to 4 days) a second VYNS film was layed down on top of the BaF_2 crystals.

The BaF_2 thin film was tested in exactly the same manner as described for the NE 102A films in Chapter 3.

Results and Discussion

The SSD, TOD, TFD and RES spectra are shown in Figures 4-1 through 4-4 respectively. The shape for all of these parameters is poorly defined and is indicative of rather serious irregularities in BaF_2 deposition. Nevertheless, the concept was shown to be valid, i.e. inorganic scintillators can be used in low energy heavy ion spectrometry. The timing resolution at fwhm was 2.17 ns which is about a factor of four higher than obtained for the NE 102A films. The shift in the TOF spectrum caused by velocity attenuation in the BaF_2 film was determined to be about 0.9 ns for the M_L peak which is the same delay caused by the 260 $\mu g/cm^2$ NE 102A film; to a first approximation, the areal density of the BaF_2 film is probably the same order of thickness.

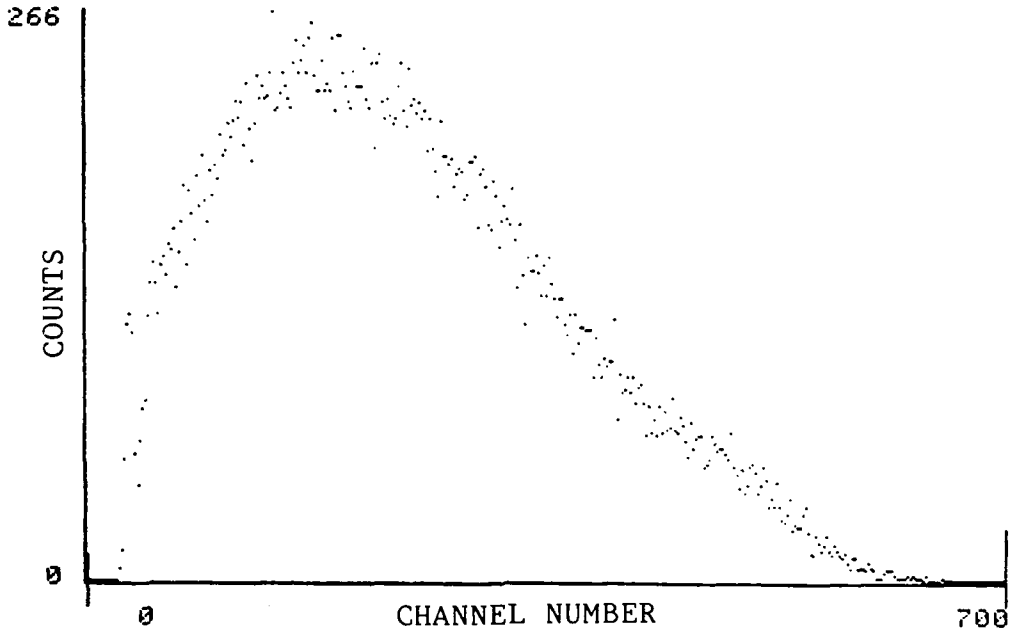

Figure 4-1 SSD spectrum with BaF_2 film inserted.

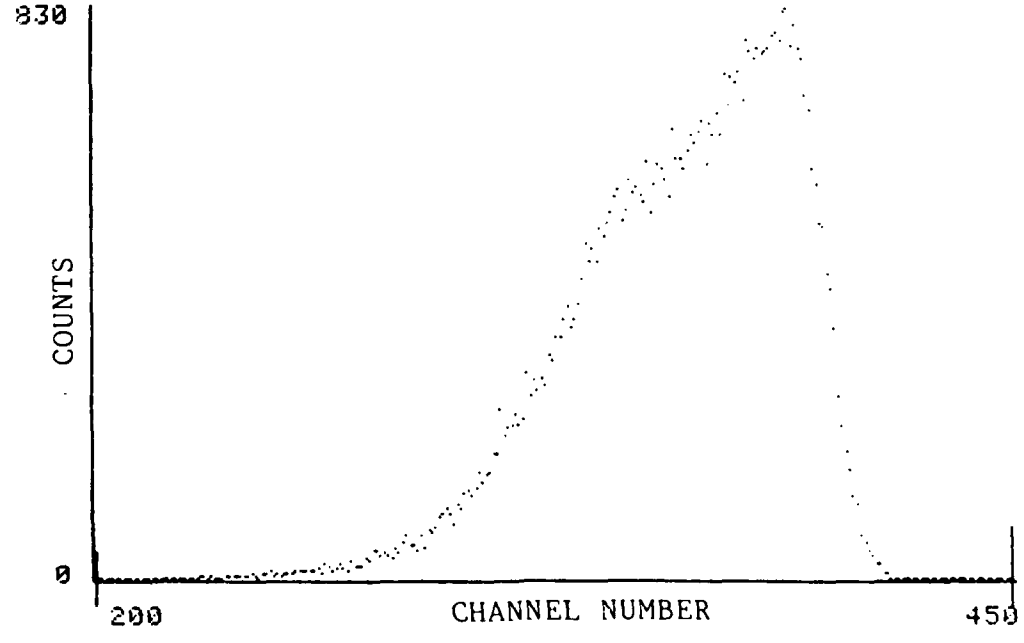

Figure 4-2 TOF spectrum with BaF_2 film inserted.

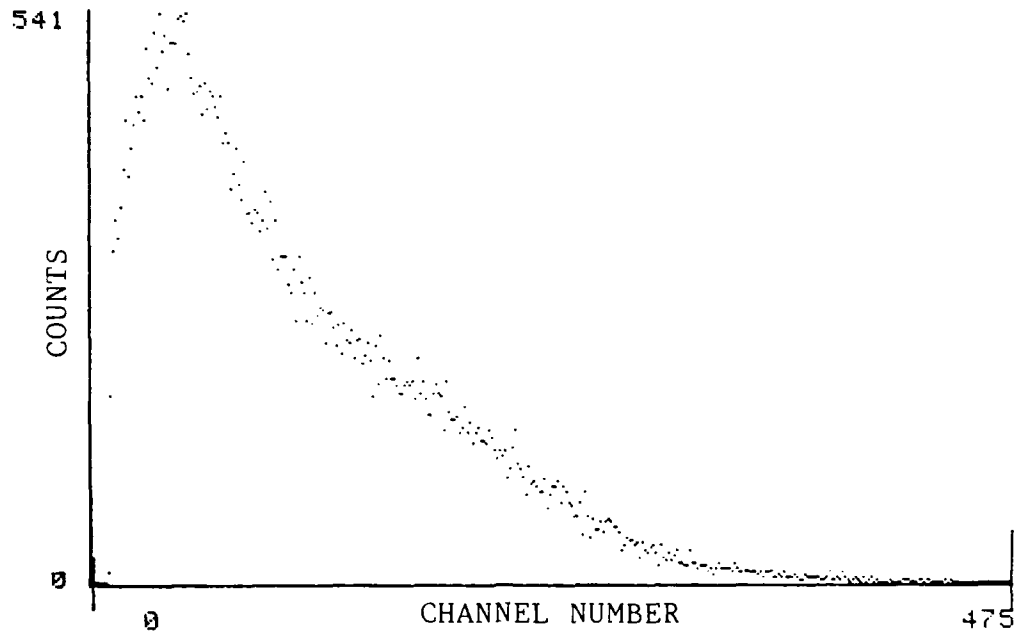

Figure 4-3 BaF_2 thin film response.

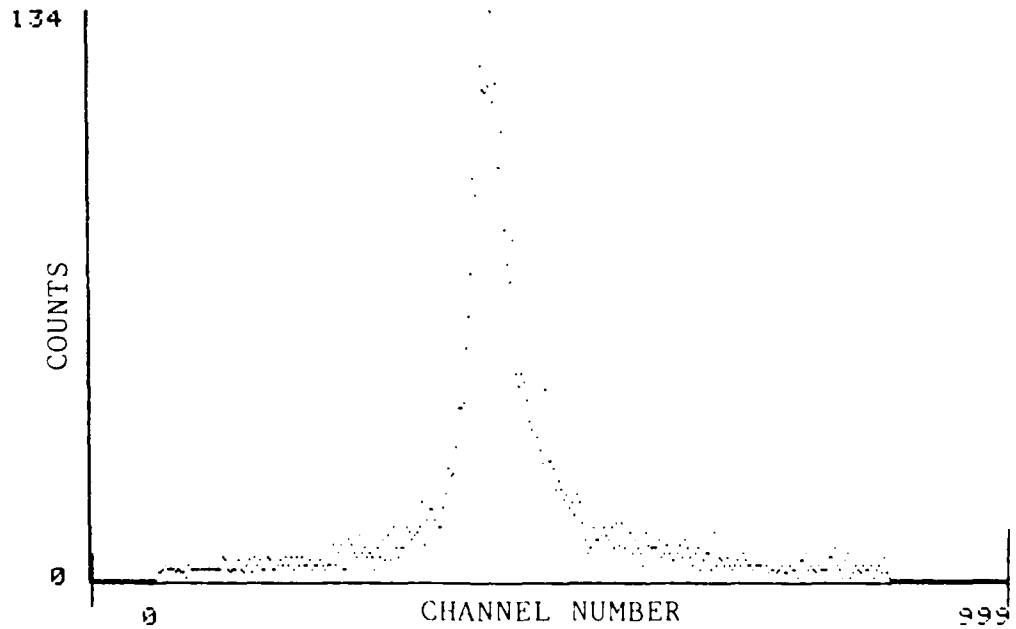

Figure 4-4 Timing resolution of BaF_2 thin film.

The M_H and M_l peaks were not resolved in any of the spectra and consequently the P/V of the TFD spectrum could not be measured. However, the relative position of the overall spectrum with regard to channel numbers, indicates a light output almost exactly between the NE 102A films of 70 $\mu g/cm^2$ and 140 $\mu g/cm^2$ thickness. This observation suggests the BaF_2 scintillator film is about half as efficient in light output as NE 102A. This is to be expected since the light output of NE 102A is reported to be about 30% that of NaI(Tl) whereas the light output for BaF_2 is only about 20% that of NaI(Tl) [67,68].

Undoubtedly significant improvements in the scintillation response are possible if a more uniform BaF_2 film can be fabricated. Preliminary experiments involving electrodeposition show great potential for developing such films.

CHAPTER 5
SUGGESTIONS FOR FURTHER WORK

If the utility of thin film systems is to continue to increase, more research must be done focussing on the chemical composition and fabrication of the thin films themselves. Experiments involving different scintillator materials need to be conducted. Since self-absorption is not a problem in thin films, plastic scintillators containing greater concentrations of fluor than available commercially need to be studied. Because the dissolving power of polymer solutions (such as the NE 102A solution studied in this thesis) is quite limited, high concentrations can only be obtained by dissolving the scintillator material in a solution of the monomer; the solution is then polymerized either chemically or by ionizing radiation to form the plastic incorporating the fluor.

Indeed, there are a great many interesting possibilities worthy of detailed study. It is hoped that this work might at least represent a small step in the right direction.

REFERENCES

1) M. L. Muga, D. J. Burnsed, W. E. Steeger and H. E. Taylor, Nucl. Instr. and Meth. 83 (1970) 135.

2) J. C. D. Milton and J. S. Fraser, Can. J. Phys. 40 (1962) 1626.

3) M. L. Muga, Nucl. Instr. and Meth. 95 (1971) 349.

4) C. K. Gelbke, K. D. Hildebrand and R. Bock, Nucl. Instr. and Meth. 95 (1971) 397.

5) T. Batsch and M. Moszynski, Nucl. Instr. and Meth. 123 (1975) 341.

6) L. Muga and D. Burnsed, Rev. Sci. Instrum. 47 (1976) 924.

7) L. Muga, Nucl. Instr. and Meth. 105 (1972) 61.

8) G. Bendiscioli, V. Filippini, C. Marciano, A. Rotondi and A. Zenoni, Nucl. Instr. and Meth. 227 (1984) 478.

9) L. Muga, A. Clem, G. Griffith, H. S. Plnedl, R. Eaker and R. Holub, Nucl. Instr. and Meth. 119 (1974) 255.

10) R. K. Batra and A. C. Shotter, Nucl. Instr. and Meth. 124 (1975) 101.

11) R. K. Batra and A. C. Shotter, Nucl. Instr. and Meth. B5 (1984) 14.

12) F. D. Brooks, W. A. Cilliers and M. S. Allie, Nucl. Instr. and Meth. A240 (1985) 338.

13) C. Manduchi, M. T. Russo-Manduchi and G. F. Segato, Nucl. Instr. and Meth. A243 (1986) 453.

14) I. Kanno and Y. Nakagome, Nucl. Instr. and Meth. A251 (1986) 108.

15) L. Muga and G. Griffith, Nucl. Instr. and Meth. 109 (1973) 289.

16) M. L. Muga, G. L. Griffith, H. W. Schmitt and H. E. Taylor, Nucl. Instr. and Meth. 111 (1973) 581.

17) L. Muga, Nucl. Instr. and Meth. 124 (1975) 541.

18) M. L. Muga and J. D. Bridges, Nucl. Instr. and Meth. 134 (1976) 143.

19) F. D. Becchetti, C. E. Thorn and M. J. Levine, Nucl. Instr. and Meth. 138 (1976) 93.

20) L. Muga and G. Griffith, Phys. Rev. B8 (1973) 4069.

21) L. Muga and G. Griffeth, Phys. Rev. B9 (1974) 3639).

22) L. Muga and M. Diksic, Nucl. Instr. and Meth. 122 (1974) 553.

23) N. N. Ajitanand, Nucl. Instr. and Meth. 143 (1977) 345.

24) I. Kanno and Y. Nakagome, Nucl. Instr. and Meth. A244 (1986) 551.

25) Obtainable from Thorn EMI Gencom, Inc. 23 Madison Road, Fairfield, NJ 07006.

26) F. D. Brooks, Nucl. Instr. and Meth. 162 (1979) 477.

27) G. Laustriat, Molecular Crystals, 4 (1968) 127.

28) L. Muga and A. Clem, Phys. Rev. C. 11 (1975) 1287.

29) P. Plischke, W. Scobel and R. Wien, Nucl. Instr. and Meth. 203 (1982) 419.

30) N. N. Ajitanand, K. N. Iyengar and S. R. S. Murthy, Nucl. Instr. and Meth. 205 (1983) 145.

31) F. E. Dunnam, ed., Continued Studies of Nuclei Far from Stability, Report to D.O.E. (University of Florida, 1986) unpublished.

32) M. L. Muga, D. J. Burnsed and W. E. Steeger, Nucl. Instr. and Meth. 104 (1972) 605.

33) Obtainable from Union Carbide Corporation, Atlanta, GA.

34) P. D. Goldstone, R. E. Malmin, F. Hopkins and P. Paul, Nucl. Instr. and Meth. 121 (1974) 353.

35) N. N. Ajitanad and K. N. Iyengar, Nucl. Instr. and Meth. 133 (1976) 71.

36) S. C. Gujrathi and L. Lessard, Nucl. Instr. and Meth. 206 (1983) 183.

37) G. Friedlander, J. W. Kennedy, E. S. Macias, and J. M. Miller, Nuclear and Radiochemistry, 3rd ed. (J. Wiley and Sons, New York, 1981).

38) H. R. Simonds and J. M. Church, eds., The Encyclopedia of Basic Materials for Plastics (Reinhold, New York, 1967).

39) J. W. T. Spinks and R. J. Woods, An Introduction to Radiation Chemistry (John Wiley and Sons, New York, 1964).

40) A. J. Swallow, Radiation Chemistry of Organic Compounds (Pergamon Press, New York, 1960).

41) A. Charlesby, Atomic Radiation and Polymers (Pergamon Press, New York, 1960).

42) F. A. Bovey, The Effects of Ionizing Radiation on Natural and Synthetic High Polymers (Interscience, New York, 1958).

43) A. Chapiro, Radiation Chemistry of Polymeric Systems (Interscience, New York, 1962).

44) G. Odian, Principles of Polymerization, 2nd Ed. (John Wiley and Sons, New York, 1981).

45) J. J. Harwood, H. H. Hausner, J. G. Morse, and W. G. Rauch, Effects of Radiation on Materials (Reinhold, New York, 1958).

46) L. A. Wall and M. Magat, J. Chim. Phys. 50 (1953) 308; Mod. Plast. 30 (1953) 111.

47) A. Chapiro, J. Durup, M. Fox, and M. Magat, Inter. Symp. Macromol. Chem., Milan-Turin (1954), Ricerca Sci. Suppl. A. (1955) 207.

48) J. Durup, J. Chim. Phys. 54 (1957) 739.

49) J. Durup, J. Polymer Sci. 30 (1958) 533.

50) M. Durup, J. Durup, F. Kieffer and M. Magat, Proc. 2nd Intern. Conf. Peaceful Uses Atomic Energy, 29 (1958) 143.

51) J. Durup, J. Chim. Phys. 56 (1959) 873.

52) A. Henglein and C. Schneider, Z. Physik. Chem. 18 (1958) 56.

53) A. Henglein, K. Heine, W. Hoffmeister, W. Schnabel, C. Schneider and H. Uri, Proc. 2nd Intern. Conf. Peaceful Uses Atomic Energy 29 (1958) 206.

54) I. K. Chernova, S. S. Lechchenko, V. P. Golikov and V. L. Karpov, Vysokomol. Soyed. Ser. A22 (1980) 2175.

55) R. J. Hanrahan, Int. J. Appl. Radiat. Isotopes, 13 (1962) 254.

56) A. K. Gupta and R. J. Hanrahan, The Radiolysis of Washed Tetraphenylborate Slurry Containing Na^+, OH^-, NO_2^-, and NO_3^- Ions, Report 4 (University of Florida, 1985) unpublished.

57) J. Weiss, A. O. Allen and H. A. Schwarz, Proc. Intern. Conf. Peaceful Uses Atomic Energy, 14 (1956) 179.

58) P. J. Flory, Principles of Polymer Chemistry (Cornell University Press, Ithaca, 1953).

59) H. Morawetz, Macromolecules in Solution (Interscience, New York, 1965).

60) L. H. Peebles, Jr., Molecular Weight Distributions in Polymers (Interscience, New York, 1971).

61) A. R. Schultz, P. I. Roth and G. B. Rathmann, J. Polymer Sci. 22 (1956) 495.

62) A. Charlesby, Proc. Roy. Soc. A222 (1954) 542.

63) J. Brandrup and E. H. Immergut, eds., Polymer Handbook, 2nd Ed. (John Wiley and Sons, New York, 1975).

64) V. P. Budtov and V. M. Belyayev, Vysokomol. Soyed. A12 (1970) 1909.

65) H. W. Schmitt, W. E. Kiker, and C. W. Williams, Phys. Rev. B137 (1965) 837.

66) J. S. Fraser, J. C. D. Milton, H. R. Bowman and S. G. Thompson, Can. J. Phys. 41 (1963) 2080.

67) M. Laval, M. Moszynski, R. Allemand, E. Cormoreche, P. Guinet, R. Odru and J. Vacher, Nucl. Inst. and Meth. 206 (1983) 169.

68) E. Nardi, Nucl. Instr. and Meth. 95 (1971) 229.

BIOGRAPHICAL SKETCH

Steven Dane Thompson was born in Pensacola, Florida, on September 17, 1962. He graduated from Tate High School in 1980. He received an Associate of Arts degree from Pensacola Junior College in 1982, and graduated in 1984 from the University of West Florida with a Bachelor of Science degree in chemistry. On November 30, 1984, he was commissioned a Second Lieutenant in the United States Air Force after successful completion of Officer Training School at San Antonio, Texas. He entered the University of Florida Graduate School in the fall of 1986.

He is married to the former Lee Ann Parker. Their only son, Justin Steven, was born on November 26, 1986.